Resolving the origin of pseudo-single domain magnetic behavior

Andrew P. Roberts[1], Trevor P. Almeida[2], Nathan S. Church[3], Richard J. Harrison[4], David Heslop[1], Yiliang Li[5], Jinhua Li[6], Adrian R. Muxworthy[7], Wyn Williams[8], and Xiang Zhao[1]

1. Research School of Earth Sciences, The Australian National University, Canberra, ACT 2601, Australia

2. School of Physics and Astronomy, University of Glasgow, Glasgow, G12 8QQ, UK

3. Department of Geoscience and Petroleum, Norwegian University of Science and Technology, Trondheim, Norway

4. Department of Earth Sciences, University of Cambridge, Cambridge, CB2 3EQ, UK

5. Department of Earth Sciences, The University of Hong Kong, Hong Kong, Pokfulam Road, China

6. Key Laboratory of Earth and Planetary Physics, Institute of Geology and Geophysics, Chinese Academy of Sciences, Beijing 100029, China

7. Department of Earth Science and Engineering, Imperial College London, South Kensington Campus, London, SW7 2AZ, UK

8. Grant Institute of Earth Science, University of Edinburgh, Kings Buildings, West Mains Road, Edinburgh, EH9 3JW, UK

This article has been accepted for publication and undergone full peer review but has not been through the copyediting, typesetting, pagination and proofreading process which may lead to differences between this version and the Version of Record. Please cite this article as doi: 10.1002/2017JB014860

Abstract

The term ‘pseudo-single domain’ (PSD) has been used to describe the transitional state in rock magnetism that spans the particle size range between the single domain (SD) and multi-domain (MD) states. The particle size range for the stable SD state in the most commonly occurring terrestrial magnetic mineral, magnetite, is so narrow (~20-75 nm) that it is widely considered that much of the paleomagnetic record of interest is carried by ‘PSD’ rather than stable SD particles. The PSD concept has, thus, become the dominant explanation for the magnetization associated with a major fraction of particles that record paleomagnetic signals throughout geological time. In this paper, we argue that in contrast to the SD and MD states, the term ‘PSD’ does not describe the relevant physical processes, which have been documented extensively using three-dimensional micromagnetic modeling, and by parallel research in materials science and solid-state physics. We also argue that features attributed to ‘PSD’ behavior can be explained by nucleation of a single magnetic vortex immediately above the maximum stable SD transition size. With increasing particle size, multiple vortices, antivortices, and domain walls can nucleate, which produce variable cancellation of magnetic moments and a gradual transition into the MD state. Thus, while the term ‘PSD’ describes a well-known transitional state, it fails to describe adequately the physics of the relevant processes. We recommend that use of this term should be discontinued in favor of “vortex state”, which spans a range of behaviors associated with magnetic vortices.

1. Introduction

More than 55 years have passed since *Stacey* [1961, 1962] coined the term 'pseudo-single domain' (PSD) to describe a transitional magnetic state between the stable single domain (SD) and multi-domain (MD) states. SD particles are uniformly magnetized; when they occur above the lower threshold size at which they have thermal stability, they can retain a record of the magnetic field in which they were magnetized for durations that exceed the age of the Earth [*Néel*, 1949, 1955]. This extraordinary recording capability has made paleomagnetism widely useful in understanding Earth (and solar system) history, particularly through establishment of the geomagnetic polarity timescale and the plate tectonic paradigm. However, the stable SD state occurs over only a narrow range of particle sizes in magnetite (~20-75 nm for equant particles at room temperature, with an upper threshold size of ~200 nm for elongated particles with 2:1 axial ratios [*Muxworthy and Williams*, 2009]). In order to minimize the total magnetic energy within and on the surface of a particle, the dominant demagnetization energy drives larger particles to subdivide into magnetic domains, with narrow domain walls between domains. In the MD state, the magnetic moment per unit volume is much lower than for SD particles because the magnetic moments of domains largely cancel each other. MD particles are generally not paleomagnetically stable on geological timescales [e.g., *Heider et al*., 1988]. SD behavior is, therefore, far more desirable for providing reliable paleomagnetic recording.

Instead of observing a sharp transition between the SD and MD states that reflects their markedly contrasting magnetic properties, a gradual transition is observed above the upper threshold size for stable SD behavior [*Verhoogen*, 1959; *Stacey*, 1961, 1962, 1963], with true MD behavior often not observed in magnetite until particle sizes above 20-25 μm [*Vlag et al*., 1996] or even 100 μm [*Heider et al*., 1996]. The particle size range over which this transition occurs depends on the spontaneous magnetization, shape, and the state of internal stress of a particle [e.g., *Day et al.*, 1977; *Heider et al*., 1987; *Dunlop and Özdemir*, 1997]. Manifestations of PSD behavior include gradual

variation of the ratio of the saturation remanent magnetization (M_{rs}) to saturation magnetization (M_s) and coercive force (B_c) across a broad particle size range (Figure 1) rather than decreasing sharply at the upper threshold size for stable SD behavior. These parameters have intermediate values between ideal SD and MD values.

The importance of the so-called PSD state in paleomagnetism, rock magnetism, and environmental magnetism is difficult to overstate. The fact that stable paleomagnetic behavior is preserved across a much larger particle size range than the narrow SD size range makes paleomagnetism useful for addressing wide-ranging geoscientific problems. The paleomagnetic importance of particles in this larger size range has long been recognized and the origin of PSD behavior has been much-debated for over 50 years [e.g., *Verhoogen*, 1959; *Stacey*, 1961, 1962, 1963; *Banerjee*, 1977; *Day*, 1977; *Dunlop*, 1977, 1981, 1986; *Levi and Merrill*, 1978; *Moskowitz*, 1980; *Halgedahl and Fuller*, 1983; *Fuller*, 1984; *Halgedahl*, 1987; *Enkin and Dunlop*, 1987; *Xu and Dunlop*, 1993; *Williams and Dunlop*, 1995; *Pokhil and Moskowitz*, 1997; *Fabian and Hubert*, 1999]. The importance of stable magnetizations in this transitional particle size range makes it unsatisfactory for the origin of PSD behavior to remain uncertain. Below, we provide an historical overview of explanations for PSD behavior, along with key observations that must be explained to account for PSD behavior (Section 2). This is followed by presentation of key pieces of evidence that we argue provide a convincing physical explanation for 'PSD' behavior.

In terms of the motivation for this paper, we note that the PSD state was hypothesized at about the same time that two-dimensional (2D) micromagnetic models became available, but long before three-dimensional (3D) models were applied in a rock magnetic context [*Williams and Dunlop*, 1989]. For example, from micromagnetic considerations it has long been recognized in materials science and solid-state physics that when particles are larger than the stable SD size, their magnetization no longer reverses in response to an applied field via coherent rotation as envisaged in the *Stoner and Wohlfarth* [1948] model. Instead, in 'soft' ferrimagnetic materials with relatively weak magnetocrystalline

anisotropy a "curling" mode of magnetization reversal occurs in which the magnetization curls around a central axis [*Frei et al*., 1957; *Brown*, 1957, 1958; *Luborsky*, 1961]. This magnetization reversal mode was later referred to as the vortex state when the first 3D micromagnetic modeling was undertaken [*Schabes and Bertram*, 1988]. A magnetization state known as the "flower" state develops before nucleation of the vortex state, where magnetic moments spread outward at the edges of a particle [*Schabes and Bertram*, 1988]; for the purposes of this paper, we treat the flower state as representing the coarse-grained end of the stable SD state because the magnetization remains essentially uniform at the center of the particle. While the flower state departs from the purely uniform SD state of *Néel* [1949], such particles have recently been shown to have slightly increased thermal and field stability with respect to true SD particles [*Nagy et al*., 2017]. Once a flower state is no longer stable, a characteristic of the vortex state is that the magnetization reverses by discontinuous jumps at given nucleation fields [*Luborsky*, 1961]. While elements of this reasoning are embedded in the rock magnetic literature, divergent thinking has arisen between the materials science/solid state physics and rock magnetic communities concerning the nature of the SD-MD transition. Soon after the first 3D micromagnetic models were produced in a rock magnetic context [*Williams and Dunlop*, 1989], which included recognition of the curling mode of magnetization, specific micromagnetic tests of 'PSD' behavior were conducted [*Williams and Dunlop*, 1995; *Fabian et al*., 1996; *Rave et al*., 1998; *Newell and Merrill*, 2000]. These studies confirmed that the stable magnetizations observed for 'PSD' particles result from nucleation of vortex states. Although this explanation has been accepted by some paleomagnetists [e.g., *Tauxe et al*., 2002], it has not been accepted universally in the paleomagnetism community despite widespread appreciation of information derived from micromagnetic simulations. For example, *Dunlop* [2002] referred to the vortex state as exotic and argued that experimental observations of 'PSD' behavior can be explained by mixtures of SD and MD states. Thus, disagreement about the origin of the 'PSD' state has persisted and the term 'pseudo-single domain' remains embedded in the literature.

Experimental understanding of the magnetic behavior associated with the 'PSD' state has been problematic. Standard methods that are used to synthesize magnetic particles for fundamental rock magnetic analysis (e.g., hydrothermal, glass-ceramic) usually produce samples with broad particle size distributions, with little or no control of inter-particle spacing so that magnetostatic interactions have been a significant complicating factor in resulting magnetic characterizations. This has made it impossible to isolate and study 'PSD' behavior in the bulk samples used in paleomagnetic studies. Electron beam lithography (EBL) has been used to address this problem by producing arrays of identical magnetic particles with controlled spacing [*King et al*., 1996; *Krása et al*., 2009]. These studies have been helpful in studying 'PSD' behavior; however, production of samples by EBL has also proven to be difficult, with only a few non-ideal samples produced, where the samples are often affected by induced stress related to the sample/substrate interface.

Domain state imaging has been a key tool for understanding the magnetic properties of coarser particles in rock magnetism. However, direct imaging of vortex structures in < 500 nm particles has been historically difficult for two reasons. First, vortex structures have small external fields. This makes them difficult or impossible [*Williams et al*., 1992] to image with the dominantly used domain imaging methods like Bitter pattern imaging and magnetic force microscopy that rely on stray surface fields [e.g., *Soffel*, 1977; *Halgedahl and Fuller*, 1980; *Heider et al*., 1988; *Moskowitz et al*., 1988; *Halgedahl*, 1991; *Pokhil and Moskowitz*, 1997; *de Groot et al*., 2014]. Second, particles in this size range are difficult to resolve with light microscopy, which is used in Bitter pattern imaging. Development and application of advanced transmission electron microscope (TEM) techniques such as off-axis electron holography now make it possible to image directly magnetic structures at nanometer scales [*Cowley*, 1992], although the resulting 2D images can lead to ambiguity in determining 3D structures [*Almeida et al*., 2016]. Nevertheless, electron holography has proven to be an exceptionally useful tool in understanding complexities associated with various types of mineral magnetic microstructures [e.g., *Dunin-Borkowski et al*., 1998; *Harrison et al*., 2002; *Almeida et al*.,

2014; *Einsle et al*., 2016]. Recently developed 3D hard X-ray magnetic imaging [*Donnelly et al*., 2017] has yet to be used in rock magnetism, but promises to open new avenues for understanding magnetic structures of relevance to rock magnetism.

In this paper, we combine evidence from first-order reversal curve (FORC) diagrams [*Pike et al*., 1999; *Roberts et al*., 2000], which provide information about all components of magnetization in a sample, with support from numerical micromagnetic simulations and electron holography, to seek to explain the physics of magnetization processes associated with the 'PSD' state. We present observations that confirm that the 'PSD' state has been misdiagnosed routinely in paleomagnetism and rock magnetism and that the key observations that must be explained to account satisfactorily for 'PSD' behavior (see Section 2) can be explained by magnetically non-uniform single and multiple vortex states with domain wall nucleation at coarser particle sizes.

2. Historical overview and key observations of PSD behavior

Dunlop and Özdemir [1997] provide an extensive description of the PSD state to which readers are directed for a comprehensive account. *Fabian and Hubert* [1999] also provide an excellent concise summary of key concepts associated with development of attempts to explain 'PSD' behavior. We provide a brief overview below to trace the major concepts, but also to describe the key observations that must be accounted for in any successful explanation of magnetic behavior across the extended particle size range over which 'PSD' behavior occurs.

Even before the term 'PSD' was coined, *Verhoogen* [1959] proposed that stable remanences in large particles could be explained by SD inclusions due to deflected electron spins surrounding local stress concentrations or dislocations within MD grains. *Stacey* [1961] argued that even if SD regions existed within MD particles, they would be magnetically screened so that MD properties would still dominate. Instead, *Stacey* [1962] argued that permanent PSD moments could be explained by 'Barkhausen discreteness' where changes in remanence occur as a result of Barkhausen jumps of

domain walls between positions that are magnetoelastically bound to defects. In this case, domain walls will not annihilate fully the total magnetic moment and an uncompensated PSD moment was argued to result. PSD moments were not considered to be independent of MD processes in these early models [*Dunlop and Özdemir*, 1997]; later explanations emphasized true SD moments within PSD particles, where SD moments can reverse independently of surrounding domains [*Dunlop*, 1973, 1977] or where domain walls fail to renucleate after magnetic saturation is achieved in metastable SD grains [*Halgedahl and Fuller*, 1980, 1983]. The possibility of domain wall moments (referred to as PSARKs), where PSD remanence results from magnetization structures within domain walls [*Dunlop*, 1977], fails to account for the grain size dependence of the saturation remanence. Domain imbalance in particles with irregular shape [*Stacey*, 1961] or odd numbers of domains [*Scherbakov*, 1978], have been argued to give rise to PSD effects [*Dunlop*, 1983]. However, domain imbalance moments vanish for small particles that still preserve a significant PSD remanence. Surface anisotropy was proposed by *Banerjee* [1977] to explain high coercivities in PSD particles. However, such surface moments interact strongly with the volume magnetization, which is incompatible with the expected grain size dependence (as is the case for the wall moment hypothesis).

Unconstrained 3D micromagnetic models provide a powerful means of visualizing inhomogeneous magnetizations at sub-micron length scales. At fine particle sizes, simple, uniform SD structures are observed. As particle size increases, flower (Figure 2a) and vortex structures (Figure 2b, c) form above the stable SD threshold size [*Schabes and Bertram*, 1988; *Williams and Dunlop*, 1989, 1995; *Enkin and Williams*, 1994; *Fabian et al*., 1996; *Rave et al*., 1998; *Newell and Merrill*, 2000]. Coercivity predictions from 3D micromagnetic models agree well with experimental data for unstressed cubic magnetite particles, although the saturation remanence is lower than expected [*Williams and Dunlop*, 1995]. Vortex-like structures are the equilibrium or lowest energy state for non-uniformly magnetized particles in 3D micromagnetic calculations [*Williams and Dunlop*, 1995]. Close agreement between micromagnetic theory and experimental data for ‘PSD’ particles has led to

the suggestion that metastable vortex states, which have high magnetic moment and coercivity, are the dominant magnetization state in small 'PSD' particles, with magnetization reversal controlled by vortex nucleation and propagation [*Williams and Dunlop*, 1995]. In this paper, we provide evidence in support of this conclusion.

In seeking to explain PSD behavior, we bear in mind the comments of *Fabian and Hubert* [1999] who stated that any explanation needs to account for the universality of PSD remanence in all kinds of magnetic materials across a broad transitional size range, the high intensity of a weak-field thermal remanent magnetization (TRM) above the theoretically predicted SD threshold size, and the coercivity spectrum of a weak-field TRM that is similar to that of a mixture of SD and MD components. A key manifestation of SD-like and MD-like components in PSD magnetite is low-temperature demagnetization (LTD) in magnetite when it is cooled through the isotropic temperature (130 K) and Verwey transition (120 K) [*Verwey*, 1939]. The remanence fraction that survives LTD, or the low-temperature (LT) memory, has SD-like behavior during alternating field (AF) demagnetization, whereas that removed during LTD has MD-like behavior [*Ozima et al*., 1964]. *Fabian and Hubert* [1999] concluded that any explanation for PSD behavior should have a simple and natural explanation that accounts for the above observations. We seek to achieve this with FORC diagrams, micromagnetic simulations, and electron holography to illustrate how single and multiple vortex states, and associated phenomena, can explain 'PSD' behavior.

3. Understanding magnetic domain states using FORC diagrams

FORC diagrams [*Pike et al*., 1999; *Roberts et al*., 2000] have been used widely to understand microscopic magnetization mechanisms in geological and synthetic samples. A framework for understanding the magnetic behavior of superparamagnetic, magnetostatically interacting and non-interacting SD, MD, single vortex, and 'PSD' particle systems has been developed through experimental, theoretical, numerical, and micromagnetic approaches. *Roberts et al*. [2014] provide an

up-to-date summary and details concerning the physical meaning and interpretation of FORC diagrams. We provide here a brief outline of the manifestations of SD, MD, and 'PSD' states in FORC diagrams, including observations that suggest vortex nucleation as a credible explanation for 'PSD' behavior. This background is necessary for using FORC diagrams to explain the magnetization mechanisms responsible for 'PSD' behavior.

3.1 The SD, MD, and 'PSD' states

Non-interacting uniaxial SD particle systems produce a dominantly horizontal signature on FORC diagrams (Figure 3a). The magnitude of the FORC distribution along the horizontal axis provides a measure of the coercivity (switching field) distribution, while the sharp ridge-like distribution indicates a lack of magnetostatic interactions among the uniaxial SD particles [e.g., *Pike et al*., 1999; *Roberts et al*., 2000; *Newell*, 2005; *Muxworthy and Williams*, 2005; *Egli*, 2006; *Winklhofer and Zimanyi*, 2006; *Egli et al*., 2010; *Dobrota and Stancu*, 2013]. As interactions increase, the vertical spread of the FORC distribution increases [*Pike et al*., 1999; *Roberts et al*., 2000; *Muxworthy et al*., 2004]. By contrast, MD particle systems with weak domain wall pinning give rise to dominantly vertical FORC distributions with low coercivities [*Pike et al*., 2001; *Roberts et al*., 2014] (Figure 3b). The weak domain wall pinning regime is approximated by the domain wall pinning model of *Néel* [1955], where planar domain walls do not interact magnetically with each other [*Pike et al*., 2001]. Experimental results for natural samples indicate that internal stress is important and that it gives rise to FORC distributions that are no longer dominantly vertical, but that diverge away from the vertical axis of FORC diagrams to higher coercivities [*Pike et al*., 2001]. In Figure 3c-f, FORC diagrams are shown for magnetite with particle size from the MD through 'PSD' size range from 76 to 7 μm [*Muxworthy and Dunlop*, 2002]. The large, unstressed 76-μm hydrothermal magnetite sample has a dominantly vertical FORC distribution similar to that for an annealed 2-mm magnetite or a non-annealed 125-μm magnetite reported by *Pike et al*. [2001]. As particle size decreases, the FORC

distributions have increasing coercivities with progressively greater divergence from the B_i axis. For the finest-grained sample, the peak of the distribution almost closes onto a SD-like peak. *Roberts et al*. [2000] and *Muxworthy and Dunlop* [2002] reported that PSD grains have a combination of MD-like moments with both diverging contours and closed SD-like contours. FORC diagrams such as Figure 3f are widely taken to be typical of 'PSD' behavior.

3.2 The single vortex state

The single vortex magnetic state has been investigated from numerical and experimental perspectives using FORC diagrams. *Carvallo et al*. [2003] used numerical micromagnetic modeling to simulate FORC diagrams for an elongated magnetite particle just above the stable SD threshold size (100 x 80 x 80 nm). When the magnetization decreases from saturation, it changes progressively from a stable SD state to a flower state to a vortex state, and back to a flower state and stable SD state as it approaches negative saturation. These intermediate magnetization states produce switching branches in simulated FORCs that do not always occur at the same field (Figure 4a). The different switching branches give rise to multiple positive and negative peaks in a FORC diagram (Figure 4b). This raises questions about whether a randomly oriented assemblage of such particles could give rise to multiple peaks on a FORC diagram that coalesce to form the broader spread observed in geological samples with PSD behavior (e.g., Figure 3f) as suggested by *Egli and Winklhofer* [2014] and *Roberts et al*. [2014]. Micromagnetic simulation of such realistic assemblages remains computationally prohibitive, but we present results below for a single particle. Before presenting these simulation results, we describe the manifestations of vortex states in FORC diagrams from simple model simulations.

Pike and Fernandez [1999] investigated the single vortex state within arrays of cobalt dots (with dimensions of 260 x 450 x 30 nm). They reported FORC diagrams with 3 prominent features associated with single vortex nucleation and annihilation (Figure 4c), with magnetization switching represented by simplified truncated square hysteresis loops known as hysterons (e.g., Figure 4d, e).

Hysterons are idealized hysteresis loops where the applied field is parallel to the easy axis of magnetization of uniaxial SD particles. Hysterons are used widely to understand SD particle systems and to illustrate the manifestation of magnetic switching due to coherent rotation of magnetization in FORC diagrams, where the single switching event in a hysteron produces a single point response in a FORC diagram (Figure 4f) [*Roberts et al*., 2000; 2014]. In reality, the magnetization depends on the angle of the applied field to the easy axis of a SD particle. The *Stoner and Wohlfarth* [1948] model enables such an approximation of SD behavior, with rounded hysteresis loops associated with coherent rotation of magnetization with variable angle of applied field with respect to the easy axis of magnetization (Figure 4d, g). Accordingly, the FORC manifestation is not a single point response, but is more complicated with weak negative and positive regions, and a strong main peak (Figure 4h) in the same position as for the hysteron approximation (Figure 4f). *Muxworthy et al*. [2004], *Newell* [2005], and *Roberts et al*. [2014] give detailed explanations of these responses. *Pike and Fernandez* [1999] simulated vortex nucleation and annihilation using truncated hysterons (Figure 4i, k), where the magnetization switches from saturation by forming a vortex at a given nucleation field (B_N) that annihilates at about the same negative applied field ($-B_A$). For the ascending FORC, a vortex nucleates at a given negative field ($-B_N$) and annihilates at about the same positive applied field (B_A). In this representation, two positive peaks occur in the upper and lower half planes of the FORC diagram (Figure 4j, l), where the B_c and B_i coordinates of the peaks depend on the vortex nucleation/annihilation fields with $B_c = (B_A-B_N)/2$ and $B_i = \pm (B_A+B_N)/2$ [*Pike and Fernandez*, 1999] (Figure 4i, k). *Pike and Fernandez* [1999] also simulated a weaker "butterfly" feature along the $B_i = 0$ axis that consists of a circular negative region with a superimposed elongated horizontal positive region (Figure 4c). A vortex will not necessarily annihilate at the same field magnitude at which it nucleated; this possibility becomes more likely if physical irregularities occur within a particle. The butterfly feature along the horizontal axis results from two distinct annihilation fields [*Pike and Fernandez*, 1999], and will not be present if this condition is not met. Vertical spreading of peaks in

the lower and upper half planes of the FORC diagram reflects the distribution of nucleation/annihilation fields. *Pike and Fernandez* [1999] presented experimental FORC diagrams similar to Figure 4c for arrays of cobalt dots produced by interference lithography.

The observations of *Pike and Fernandez* [1999] have been confirmed for <100 nm iron nanodots [*Dumas et al.*, 2007a, b]. For 52 nm nanodots, non-interacting SD behavior is observed (Figure 4m) with a negative region near the B_i axis (e.g., Figure 4h). As the iron nanodots increase to 58 nm, single vortex behavior appears (Figure 4n), as observed by *Pike and Fernandez* [1999] (Figure 4c). When the dot size increases to 67 nm, the magnitude of the major peaks and the distance of the peaks from the B_i = 0 axis (i.e., the nucleation/annihilation field) increases (Figure 4o), and a "butterfly" feature appears. These results illustrate clearly the effects of vortex nucleation/annihilation on FORC diagrams for samples with precisely controlled particle size.

3.3 The vortex state and 'PSD' behavior

Despite the simplicity of the numerical model used by *Pike and Fernandez* [1999] to represent the single vortex state, it replicates key aspects of experimental results for synthetic samples with tightly controlled magnetic particle size [*Dumas et al*., 2007a, b]. The observation that the vertical separation between the upper and lower peaks of the FORC distribution depends on the magnitude of vortex nucleation/annihilation fields raises questions about whether a broader distribution of single vortex nucleation/annihilation fields associated with broader particle size distributions could give rise to the FORC diagrams observed for geological samples with 'PSD' behavior (e.g., Figure 3f). We explore this possibility using several examples in Figure 5.

FORC diagrams for geological samples routinely provide evidence of 'PSD' behavior as in Figure 3f and do not often contain evidence of single vortex states as illustrated in Figure 4c, n, o. An exception is shown in Figure 5a in which single vortex behavior is clear in a conventional FORC diagram (from *Zhao et al*. [2017]). The sample in question is an extracellular magnetite [*Li*, 2012]

produced by thermophilic iron-reducing bacteria (*Thermobacter* spp. strain TOR39), which occur as hexagonal plates (Figure 5d-f). Importantly, the plates have a relatively constant thickness and a relatively narrow particle size distribution across several hundred nm, which is within the size range expected for 'PSD' behavior [*Muxworthy and Williams*, 2009]. It is the relatively narrow particle size distribution of this sample that gives rise to the clear single vortex FORC distribution in Figure 5a, although magnetostatic interactions associated with packing of the magnetite particles will have produced additional vertical spreading of the FORC distribution.

As demonstrated by *Zhao et al.* [2017], using a new FORC measurement type that includes transient-magnetization-free measurements, we can isolate the effect of transient magnetization processes due to self-demagnetization in coarse-grained magnetic particles. The transient magnetization is the magnetization difference between the upper and lower branches of a minor hysteresis loop between the saturating field and zero-field [*Fabian*, 2003]. When the magnetization decreases from saturation, it is controlled by both field-driven magnetization changes and transient processes. The transient magnetization will decay to zero when the applied field returns to zero and will stay at zero even if the field increases [*Fabian*, 2003]. Thus, when the magnetization is measured from zero-field to saturation (referred to as the zero-FORC by *Yu and Tauxe* [2005]), only field-driven (i.e., transient-free) magnetization reversal occurs. By measuring a series of zero-FORCs within a conventional set of FORC measurements following the procedure of *Zhao et al*. [2017], it is possible to determine a FORC distribution for the transient-free magnetization component (Figure 5b). Then, by subtracting the transient-free FORC (tfFORC) distribution from the conventional FORC distribution, it is possible to obtain the FORC distribution due to the transient magnetization component (Figure 5c). Thus, the transient FORC (tFORC) diagram [*Zhao et al*., 2017] provides a measure of the distributions of nucleation and annihilation fields of magnetic vortices and domains. In the tFORC diagram for the *Thermobacter* magnetite in Figure 5c, the peaks above and below the B_i = 0 axis reflect the distribution of nucleation and annihilation fields of magnetic vortices associated with

the particle size distribution illustrated in Figure 5d-f. Interpretation in terms of vortex nucleation and annihilation follows naturally from the discussion above about the manifestations of single vortex behavior in FORC diagrams (Figure 4). These peaks are evident in the conventional FORC diagram for the *Thermobacter* magnetite (Figure 5a), but they are not evident in conventional FORC diagrams for typical geological samples that contain 'PSD' magnetic particles. Transient FORC diagrams are, therefore, a powerful tool for assessing the origin of 'PSD' behavior in natural samples.

A more typical 'PSD' FORC diagram is shown in Figure 5g for an andesite sample from Mt Ruapehu, New Zealand [*Ingham et al*., 2017]. This conventional FORC diagram is not obviously representative of single vortex behavior (compare Figures 3f and 5g with Figure 4n, o). However, the characteristic vortex nucleation and annihilation field distributions above and below the $B_i = 0$ axis become evident in a corresponding tFORC diagram (Figure 5i). The vortex signature is not evident in conventional FORC diagrams because they include contributions from many magnetization processes, including remanent, induced, and transient magnetization components [*Zhao et al*., 2017]. In contrast, tFORC diagrams contain contributions from only the transient magnetization processes described by *Fabian* [2003], which provides clear evidence of magnetic vortex states without being masked by co-existing magnetization processes [*Zhao et al*., 2017]. Routine determination of tFORC diagrams [*Zhao et al*., 2017] should lead to more frequent diagnosis of 'PSD' behavior as due to vortex states. In promoting tFORC diagrams, we understand that the potential exists for false diagnosis of the vortex state. For example, when a magnetofossil chain, produced originally by magnetotactic bacteria, collapses, the magnetic flux associated with individual particles can link to create a super-vortex-like structure that would be manifest as a vortex signature in a FORC diagram [*Egli and Winklhofer*, 2014]. The extent of vortex state magnetizations in geological materials can be assessed by use of samples that do not contain magnetofossils, as will be shown in forthcoming work.

Published demonstrations of single vortex states in conventional FORC diagrams for geological samples remain non-existent to our knowledge. *Lappe et al*. [2011, 2013] reported single

vortex FORC features for synthetic dusty olivine samples. A non-interacting SD component may obscure some of the features observed in the FORC model results of *Pike and Fernandez* [1999], but the lower part of the "butterfly" feature is preserved, along with the main positive FORC features expected for single vortex behavior (these features were originally attributed to PSD behavior [*Lappe et al*., 2011], but were later attributed to single vortex behavior [*Lappe et al*., 2013]). Both stable SD and single vortex states are observed by electron holography [*Lappe et al*., 2011] in particles that span a continuous grain size distribution. This provides confirmation that single vortex nucleation and annihilation can explain important aspects of PSD behavior.

3.4 MD behavior contrasted with coarse vortex state behavior

A conventional FORC diagram for a 120-μm natural magnetite sample is shown in Figure 5j. The divergent contours are characteristic of MD behavior [*Pike et al*., 2001]. In a tFORC diagram (Figure 5l), the upper and lower parts of the distribution have a "winged" structure [*Zhao et al*., 2017] where the peaks of the distribution of domain nucleation/annihilation fields lie near the origin of the FORC diagram and the distribution intersects the $B_c = 0$ axis. This behavior contrasts with the lobate tFORC distributions in Figure 5c, i, where the lobes are indicative of vortex nucleation/annihilation fields. In Figure 5c, FORC contours close around the lobes, whereas in Figure 5l the MD contours diverge away from the origin. These contrasting features could be useful for distinguishing the extent of coexisting single vortex and domain walls. For example, the lobate features in Figure 5i close around each other, but the outer parts of the tFORC distribution also diverge away from the lobes, particularly in the lower FORC half plane. This could be evidence of combined vortex/domain wall behavior within the same particles, which is suggested by micromagnetic simulations (e.g., Figure 2c, d). The transition from the coarsest part of the vortex state to the MD state is discussed further below.

3.5 Micromagnetic simulation of the single vortex state

We now present results of numerical simulations to further illustrate how vortex states can explain 'PSD' behavior. To approximate magnetic behavior in the magnetite plates illustrated in Figure 5d-f, we simulated hysteresis behavior micromagnetically for a circular magnetite disk with 240 nm diameter and 40 nm height (Figure 6a, b) and easy axis of magnetization in the plane of the disk. Calculations were made using the Micromagnetic Earth Related Rapid Interpreted Language Laboratory (MERRILL) code, in which finite element/ boundary element methods are used to solve for the magnetic scalar potential inside a particle to calculate the demagnetizing energy, to sum the exchange, cubic anisotropy, magnetostatic, and demagnetizing energies, and to minimize the total free magnetic energy. Energy minimization was performed using a conjugate gradient method. Material parameters used are for magnetite at 20°C. Two sets of calculations were made. First, the angular dependence of hysteresis was calculated, where an external field was applied through a range of angles from parallel to the easy axis of magnetization (0°) to perpendicular to the plate (90°) at 5° increments (Figure 6b). Hysteresis loops are presented at 15° increments in Figure 6d. This simulated disk is in the single vortex magnetic state at 20°C. The vortex core lies at the center of the particle (Figure 6c) so that all magnetic moments in the plane of the disk are balanced and the net remanent magnetization will lie along the direction of the vortex core. The vortex state persists with increasing angle of applied field with respect to the plate. Figure 6f is an average of simulated loops for the disk at 5° intervals, which was calculated by accounting for geometrical weighting over the surface of a sphere for different disk orientations with respect to the applied field. Hysteresis loops with such shapes are rarely observed in nature, but this is an average of simulations at only 19 angles; natural samples will contain many millions of particles and will, therefore, give rise to smooth, rounded bulk hysteresis loops.

Natural samples also contain magnetic particles with variable size, which was simulated in a second set of calculations for disks with 40 nm thickness and long dimension varying from 20 to 320

nm at 20 nm increments (Figure 6e). For diameters of 20-100 nm, the particle is in the SD state. A vortex state nucleates at 120 nm and persists to the maximum simulated diameter of 320 nm. The average of 16 loops for plate diameters between 20 and 320 nm is shown in Figure 6g. It is usually assumed that magnetic particles in paleomagnetic samples are distributed randomly with respect to the applied field. Particle sizes are also likely to range between tens of nm and tens of microns. Extrapolating from these limited simulations, natural samples are expected to contain magnetic particles that range from having weak remanence/low coercivity to high remanence/high coercivity, with particles in the vortex state expected to have variable remanence and coercivity (Figure 6f, g). When such particles are present in geological samples, natural particle size distributions will give rise to broad-ranging coercivity and vortex nucleation/annihilation fields. Thus, our simple micromagnetic simulations further raise the question of whether typical 'PSD' FORC diagrams (e.g., Figure 3f) can be explained by vortex state particles with broad particle size distributions. We explore this possibility with micromagnetic simulations of FORCs below.

3.6 Micromagnetic simulation of FORC diagrams for the single vortex state

We simulated FORCs micromagnetically for a 240 nm x 40 nm disk (Figure 7a, b), and calculated 75 FORCs at 5° increments between 0° (parallel to the easy axis) and 90°. Results for selected orientations are shown in Figure 7a-n and for an average of 19 simulated orientations in Figure 7p. For all orientations except at 90°, the most important feature is a strong pair of positive peaks in both the upper and lower FORC half planes that are approximately equidistant from the B_i = 0 axis. The respective FORCs (Figure 7a, c, e, g, i, k, m) do not switch at a single field as in the simple hysteron-like representation in Figure 4i, k. Slight switching field variability gives rise to other features in the FORC diagrams (Figure 7b, d, f, h, j, l, n), where the main secondary features in addition to the main peaks are positive and negative distributions that extend from the main peaks back to the B_i axis at 45°. *Pike and Fernandez* [1999] explained these features as due to reversible

magnetizations associated with curved portions of FORCs that are analogous to those in the *Stoner and Wohlfarth* [1948] model (Figure 4g, h). Importantly, the main peaks in the FORC diagrams indicate that both the coercivity and strength of vortex nucleation/annihilation fields vary with applied field angle with respect to the easy axis of magnetization. These micromagnetic results, thus, provide a direct link between the physics of vortex nucleation/annihilation and expected FORC responses [*Pike and Fernandez*, 1999]. Even for so few simulations, when results for 19 orientations at 5° increments are averaged (Figure 7p), it becomes evident that averaging over a larger particle size range could get close to providing an overall bulk 'PSD'-like response (e.g., Figure 3f), as suggested by *Egli and Winklhofer* [2014] and *Roberts et al*. [2014]. However, it is likely that simulation of single vortex states alone will be insufficient and that multi-vortex features, as discussed below, will need to be included to achieve realistic simulations of bulk 'PSD'-like responses. Such a micromagnetic simulation is computationally expensive and has yet to be undertaken.

Overall, our micromagnetic results validate the simple calculations of *Pike and Fernandez* [1999] where vortex nucleation/annihilation fields produce FORC distributions that are dominated by a simple two-peak geometry. Our results are consistent with the thesis that the fine-grained end of bulk 'PSD' behavior is represented by the magnetic single vortex state.

4. Evidence for magnetic vortices from electron holography

4.1 The single vortex state

Almeida et al. [2014, 2016] published exceptionally clear off-axis electron holographic images of single vortex states in 'PSD' magnetite/maghemite with particle sizes of several hundred nm (Figure 8). The images in Figure 8 provide direct evidence of single vortex states for variable magnetite morphologies, including hexagonal particles (Figure 8c, d) similar to those in Figure 5d-f. The most important question for paleomagnetic analysis of materials in the magnetic vortex state concerns their magnetic recording capability. Single vortex state particles have been demonstrated to

have high field and thermal stability close to the Curie temperature of magnetite [*Almeida et al*., 2014, 2016; *Muxworthy et al*., 2014; *Einsle et al*., 2016; *Nagy et al*., 2017], which suggests that they are capable of recording paleomagnetic information over long geological periods. This confirms the paleomagnetic recording fidelity of 'PSD' particles that has been postulated for over 55 years.

4.2 The multi-vortex state

In addition to the single vortex state (Figure 8), multi-vortex states are evident in electron holographic images (Figure 9c, d, g, h). These images and micromagnetic simulations (Figure 9j) are for magnetite laths with widths of 100-150 nm (numbered 1-7 in Figure 9a) that are separated by titanohematite lamellae [*Church*, 2010]. The nearly pure magnetite laths and paramagnetic titanohematite lamellae ($Fe_{1.16}Ti_{0.84}O_3$) were produced synthetically by oxy-exsolution of an original titanomagnetite ($Fe_{2.4}Ti_{0.6}O_4$). A conventional FORC diagram for this sample is shown in Figure 9b, and is typical of bulk 'PSD' behavior. In addition, the FORC diagram has a superimposed "wishbone" structure that has been observed in strongly interacting Ni nanopillar arrays, where the positive peak is shifted above B_i = 0 due to a mean (negative) demagnetizing field produced by inter-particle interactions [*Pike et al*., 2005]. Magnetite lath 6 (Figure 9a) is the widest (~300 nm) and either occurs in a nearly uniformly magnetized state (Figure 9e, f, i) or with a series of stable vortices (Figure 9c, d, g, h, j) depending on the applied field. Micromagnetic simulations indicate that magnetization switching occurs by nucleation of a vortex that sweeps down the length of the lath. Also, continuous magnetic flux lines between laths indicate that this sample is affected strongly by magnetic interactions, which is also evident in the positive upward shift of the main peak in the FORC diagram. Magnetic superstates due to magnetic interactions among such exsolution features have been well documented [*Harrison et al*., 2002; *Feinberg et al*., 2006]. Regardless, this illustration demonstrates that in larger particles in the 100's of nm size range, such as magnetite lath 6, complex internal multi-vortex features occur, which indicates that the single vortex state does not transition directly into the

MD state. At these still relatively small particle sizes multi-vortex behavior becomes an important part of the spectrum of magnetic behavior associated with the 'PSD' state [*Einsle et al*., 2016]. Simulation of bulk 'PSD' FORC diagrams will, therefore, require consideration of multi-vortex behavior. Multi-vortex magnetic structures are also well known in materials science [e.g., *Harada et al*., 1996; *Ivanov et al*., 2016; *Donnelly et al*., 2017].

4.3 Other magnetic structures associated with the vortex state

As particle size increases, further phenomena must be considered to understand magnetization structures within magnetic materials in the vortex state. A major limitation in understanding the roles of relevant magnetic features has been the inability to undertake 3D imaging of magnetization structures. The recent work of *Donnelly et al*. [2017] opens the possibility of imaging the 3D magnetization state in micron-scale particles of interest for understanding the magnetic vortex state in rock magnetism. *Donnelly et al*. [2017] documented various magnetic structures that will need to be considered to develop a detailed understanding of the vortex state. For example, they demonstrated the existence of vortices with clockwise and anticlockwise vorticity. The magnetization is almost uniform between such structures with opposite vorticity, but antivortices occur in magnetically inhomogeneous regions between vortices with the same vorticity. Sequences of vortex and anti-vortex structures give rise to cross tie walls that extend through a magnetic material and separate regions with oppositely polarized magnetizations. A magnetic singularity, known as a Bloch point, can form when a vortex core intersects a domain wall. Magnetic order is destroyed at such singularities, which occur over a radius of order of the exchange length. When this range of magnetic structures can be resolved, the 3D magnetization configuration is complex for particles that span the vortex state. While many new things will be learned with application of such new techniques, the observations of *Donnelly et al*. [2017] strengthen our case for referring to the 'PSD' state as the vortex state because the complex

magnetization structures that they documented are associated with magnetic vortices and their interactions within a magnetic material.

5. Discussion

We have provided evidence that the 'PSD' state can be explained by the magnetic vortex state based on FORC diagrams, micromagnetic simulations, and electron holography. However, key aspects of 'PSD' behavior need further explanation, including the nature of the transitions from the stable SD to the single vortex state and from the multi-vortex to the MD state, along with issues mentioned by *Fabian and Hubert* [1999] as indicated in Section 2. We provide such explanations below.

5.1 Transition from the SD state to the single vortex state

Results from micromagnetic modeling, numerical simulation, experimental analysis of nanoparticle arrays with controlled particle size and inter-particle spacing, and natural geological/ bacterial/synthetic samples with narrow particle size ranges, all point to an immediate transition from the stable SD state (including a flower state) to a single vortex state. This transition is sharp [*Williams and Dunlop*, 1989, 1995]. For some materials such as equant iron particles, which are important in meteorites, there is no stable SD state at room temperature and particles pass directly from the superparamagnetic to the vortex or MD states [*Butler and Banerjee*, 1975; *Muxworthy and Williams*, 2015]. How, then, is the sharpness of the stable SD to single vortex transition reconciled with the gradual magnetic property variations (e.g., M_r, M_r/M_s, and B_c; Figure 1) observed through the 'PSD' size range? We explore this subject in Section 5.2.

5.2 Why do M_r *and* B_c *vary continuously with particle size in the vortex state?*

Particle size variations have frustrated domain state diagnosis in natural and synthetic samples, but they are also the likely cause of gradual magnetic property variations through the 'PSD' size

range. When the magnetic responses of particles with variable sizes and shapes are summed (typically millions of particles in a paleomagnetic sample), sharp transitions due to individual vortex state particles will be smoothed (smoothing of abrupt magnetization switching is even evident in the limited averaging in Figure 6g). Thus, even if all magnetic particles in a sample occur in a vortex state, vortex nucleation/annihilation field distributions will cause gradually varying bulk M_r, M_r/M_s, and B_c values with changes in average magnetic particle size. Randomized easy axis orientations in natural samples (Figure 6) will also contribute to smooth rather than abrupt magnetic property changes through the 'PSD' size range.

Use of tFORC diagrams [*Zhao et al*., 2017] enables isolation of the effects of vortex and domain wall nucleation/annihilation. When assessed using tFORC diagrams, typical 'PSD' systems manifest magnetic behavior associated with the vortex state (Figure 5i). Distributed particle sizes are also evident in the coercivity and nucleation/annihilation field distributions in Figure 5c, i. Even for the *Thermobacter* sample that appears to have obvious single vortex behavior in a conventional FORC diagram (Figure 5a), a significant stable SD component is present in the tfFORC diagram (Figure 5b). This is also the case for a typical 'PSD' sample (Figure 5g, h). Thus, widely documented SD-like moments in 'PSD' samples could partially be due to stable SD particles. Our ability to produce samples with narrow particle size and shape distributions is limited, which makes it difficult to rule out the presence of stable SD behavior. Documentation of widespread SD nanoparticles as inclusions within host silicates in the geological record provides support for this possibility [*Evans et al*., 1968; *Chang et al*., 2016]. FORC unmixing [*Lascu et al*., 2015; *Channell et al*., 2016] now makes it possible, along with the additional FORC measurements of *Zhao et al*. [2017], to discriminate SD, vortex, and MD moments in natural samples. Regardless of the possible presence of SD grains, particle size and shape variations are widespread in natural samples and are likely to be responsible for smooth magnetic property variations throughout the 'PSD' size range.

5.3 What controls the remanence direction in vortex state particles?

It is reasonable to ask what processes control the remanence direction for single vortex particles? *Einsle et al*. [2016] conducted the most extensive study of this question by characterizing magnetic domain states within iron particles in dusty olivine from a chondritic meteorite using focused ion beam nanotomography, electron tomography, and finite element micromagnetic models. They found that the remanence vector is controlled primarily by the magnetization of the vortex core and the sense of rotation of bulk spins. Slight irregularities in particle shape, including different sizes of corresponding crystal surface facets, can give rise to net remanences due to additional bulk spins in these regions. Such an imbalance between bulk spins in the single vortex state is illustrated in the experimental electron hologram in Fig. 8b, where the asymmetric particle shape gives rise to a much larger volume of spins on the right compared to the left of the image. This produces a net in-plane component of the total moment in addition to the out-of-plane moment due to the vortex core. Depending on the details of a particle, the total moment can be vortex core dominated, bulk dominated, or some combination of these two. Thus, some aspects of the early domain imbalance moment explanation for 'PSD' behavior [*Stacey*, 1961; *Shcherbakov*, 1978; *Dunlop*, 1983] could contribute to developing a more detailed understanding of the full range of magnetic behaviors in the vortex state. Overall, *Einsle et al*. [2016] concluded that particles in the single vortex state with high coercivity and large volume can have long-term paleomagnetic stability and can be reliable paleomagnetic recorders.

5.4 Transition from the multi-vortex state to the MD state

There has been much debate as to where 'PSD' behavior stops and true MD behavior begins [e.g., *Heider et al*., 1996; *Vlag et al*., 1996; *Dunlop and Özdemir*, 1997] even though it is acknowledged to correspond to the point at which the magnetization is controlled by the response of domains and domain walls to the internal demagnetizing field [*Dunlop*, 2002]. In the terms discussed

here, this transition corresponds to that between the multi-vortex and MD states. Three-dimensional micromagnetic model results reveal that as particle volume increases, vortex cores and domain walls coexist (e.g., Figure 2c, d) [*Muxworthy*, 2013]. *Einsle et al*. [2016] found that in particles several hundred nm across, the magnetic structure is dominated by the single vortex state, which gives way to multiple vortex and domain wall structures in larger particles with ~1 μm long axes. Vortex cores in these larger particles develop "winged" structures that protrude along directions in which domain walls nucleate (Figure 2c, d). Some multi-vortex scenarios simulated by *Einsle et al*. [2016] are similar to electron holograms in Figure 9 and to the complex magnetization structures documented by *Donnelly et al*. [2017]. The presence of both multiple vortex cores and domain walls in larger particles suggests that the vortex to MD transition is gradual. Important transient magnetization processes that are not discussed in detail here will also contribute to the bulk magnetization in particles through this size range. For example, pinning and partial switching of vortex core or domain wall positions are possible and will be responsible for transient magnetizations. Such processes are part of the spectrum associated with magnetic vortices, so we expect that vortex and domain wall nucleation/annihilation represent the fundamental first-order physical processes.

5.5 Can coarse particles with multiple vortex states be discriminated from MD particles?

Vortex nucleation/annihilation fields and coercivity decrease with increasing particle size (illustrated schematically in Figure 4i, k). The gradual nature of the transition between the vortex and MD states is particularly evident in the orientations of elongated upper and lower lobes of tFORC distributions. These lobes have decreasing nucleation/annihilation fields with increasing particle size and merge to $B_i = 0$, coercivity decreases progressively, and the FORC distribution shifts to the left and merges onto the B_i axis (compare Figure 5c, i, l). *Novosad et al*. [2001] also observed that vortex nucleation fields decrease with increasing particle size. These observations make it reasonable to ask

at which point does a particle change from a single vortex state to a multiple vortex state to the MD state? This question is not easy to answer, but we discuss it below.

When concentric contours define a nucleation/annihilation field distribution in a tFORC diagram, particles must be present in the single vortex state no matter how near the B_c and B_i axes the distribution lies. But such tFORC distributions also partially intersect the B_c axis, which indicates that MD particles are also present. This interpreted dominance of single vortex states is consistent with numerical hysteresis loop simulations for particles with multiple vortex cores, which are more MD-like than vortex-like (e.g., particle 233 of *Einsle et al*. [2016]). This interpretation is also consistent with micromagnetic simulations of equidimensional magnetite in Figure 2, which indicate a large single vortex core in a 80 nm particle, while at 300 nm the vortex core remains and domain walls have also nucleated at particular angles with respect to the vortex core. Overall, the transition from the vortex state to the true MD state appears to be gradual because of the coexistence of vortex cores and domain walls within the same particle (e.g., Figure 2c, d). The gradual nature of this transition makes it difficult to diagnose. The existence of new microscale tools for imaging magnetic structures [e.g., *Donnelly et al*., 2017] means that the important vortex state particle size range can now be subjected to the detailed 3D characterizations needed to develop a meaningful understanding of magnetization structures in such particles. This will be important in moving away from a phenomenological understanding of the 'PSD' state and toward a detailed physical understanding of the relevant magnetic structures.

5.6 Low-temperature behavior of 'PSD' magnetite

Fabian and Hubert [1999] concluded that any explanation for 'PSD' behavior should include the presence of SD-like and MD-like coercivity components in LTD results. When cycled through the Verwey transition (120 K) for magnetite [*Verwey*, 1939], where the crystal lattice of magnetite changes from a cubic to a monoclinic structure, the magnetocrystalline anisotropy increases by an

order of magnitude, which increases the SD to single vortex transition size from ~80 nm at room temperature to ~140 nm at ~100 K [*Muxworthy and Williams*, 1999].

Smirnov [2006, 2007] presented low-temperature FORC results for polycrystalline synthetic 'PSD' and MD magnetite samples (similar results were published independently by *Carvallo and Muxworthy* [2006]). From room temperature down to near 120 K, FORC diagrams are characteristic of those reported for 'PSD' magnetite at room temperature (compare Figure 10e, f with Figure 3f). Below the Verwey transition temperature, the central peak in the 'PSD' FORC distribution starts to split (Figure 10d) into separate peaks with concentric contours in the upper and lower parts of the FORC diagrams (Figure 10a-c). With decreasing temperature, the peaks separate progressively (Figure 10a-d). These low-temperature FORC diagrams resemble those associated with single vortex systems discussed above and reported by *Pike and Fernandez* [1999], *Dumas et al*. [2007a, b, 2009, 2012], *Winklhofer et al*. [2008], *Brandt et al*. [2013], and *Zhao et al*. [2017]. *Smirnov* [2006] recognized this possibility but dismissed it because the upper and lower peaks have significantly different magnitudes and because FORC diagrams for sample P1 lack the "butterfly" feature (Figure 4c) recognized by *Pike and Fernandez* [1999]. However, this asymmetry can be explained by different nucleation/annihilation fields [*Dumas et al*., 2007a, b, 2012; *Brandt et al*., 2013]. Likewise, a "butterfly" feature will only be present when there are two distinct annihilation fields [*Pike and Fernandez*, 1999], which does not appear to be the case with the samples of *Smirnov* [2006].

At face value, the low-temperature FORC results of *Smirnov* [2006] for 'PSD' magnetite are consistent with the presence of single vortex states. However, magnetic domain state interpretation for magnetite below the Verwey transition is complicated by the formation of crystallographic twin domains that control the local magnetocrystalline anisotropy. The positions of magnetic domain walls are often pinned strongly at twin boundaries [*Kasama et al*., 2013], and no lower size limit is known for which twin domains will not form. Furthermore, these twin walls have been shown through TEM observations to move within applied external magnetic fields at temperatures close to the Verwey

transition temperature [*Kasama et al*., 2010], although twin walls are static below the transition [*Kasama et al*., 2013]. Using detailed TEM and electron holographic observations, *Kasama et al*. [2013] demonstrated that vortex structures above the Verwey transition are converted into vortex-like structures that are defined by twin walls in the monoclinic phase below the transition. *Bryson et al*. [2013] simulated micromagnetically a field-induced 'freezing-in' of a vortex core by twin wall formation below the transition. 'Vortex nucleation' below the transition is due to nucleation and movement of 180° domain walls that lock into place when the magnetization aligns with twin walls. Vortex 'annihilation' then occurs when magnetic walls de-pin from twin walls. The simulations of *Bryson et al*. [2013] (their Figure 7) provide strong evidence that vortex states, including those associated with twin-induced closure domain structures, can explain the low-temperature hysteresis behavior discussed by *Smirnov* [2006, 2007]. Based on the above evidence, we conclude that the low-temperature FORC diagrams in Figure 10 reflect the dominance of the single vortex state (Figures 4, 5, 7) in the studied sample. *Dumas et al.* [2007b] observed that vortex states in Fe dots persist to low temperatures, that they are thermally activated, and that vortex nucleation/annihilation fields increase with decreasing temperatures. Magnetite seems to behave similarly (Figure 10). The results of *Carvallo and Muxworthy* [2006] and *Smirnov* [2006, 2007], coupled with the experimental and numerical insights of *Kasama et al*. [2013] and *Bryson et al*. [2013], could, therefore, provide the beginning of an understanding of the temperature dependence of the vortex state in magnetite where magnetic vortices act as a template for the location of twin walls below the Verwey transition.

Returning to the issue of LTD in 'PSD' magnetite, *Muxworthy and McClelland* [2000] assessed the causes of this phenomenon. They concluded that LTD has two main contributions due to (1) kinematic domain state reorganization, and (2) the change from cubic to monoclinic anisotropy, where some domains move and occupy new positions that lead to a lower net remanence after warming in zero-field. Their key finding is that internal stress, rather than particle size, controls the recovery mechanism so that AF demagnetization is unsatisfactory for distinguishing between MD-like

and SD-like behavior [*Muxworthy and McClelland*, 2000]. The two contributions to LTD proposed by *Muxworthy and McClelland* [2000] are explained better by TEM and electron holographic observations and micromagnetic simulations that provide strong evidence that the locations of magnetic vortices above the Verwey transition are a template for the placement of twin walls below the transition, so that their interactions can explain the preservation and recovery of remanence after cycling through the Verwey transition [*Bryson et al*., 2013; *Kasama et al*., 2013]. The above evidence, which combines bulk magnetic measurements with nanoscale experimental observations and micromagnetic simulations, provides hope that we are close to explaining key aspects of 'PSD' behavior that have remained elusive for decades.

5.7 Universality of 'PSD' behavior

Finally, *Fabian and Hubert* [1999] stated that explanations for the 'PSD' state must account for the universality of PSD remanence in all kinds of magnetic materials across a broad transitional size range. From the above treatment, based on various observations, as particle size increases above the stable SD threshold size and flower state in any magnetic material (e.g., magnetite, Fe, Co, Ni), the vortex state becomes the next stable domain state. The vortex state, therefore, provides an explanation for the universality of 'PSD' behavior. Like the terms 'single domain' and 'multidomain', the term 'vortex state' provides a description of the physics of the dominant magnetization process, which 'pseudo-single domain' does not. Thus, we recommend abandonment of 'PSD' in favor of 'vortex state'. The vortex state spans a complex and wide range of phenomena associated with magnetic vortices, including single and multiple vortices, antivortices, cross tie walls, domain walls, and Bloch points. The term 'vortex state' is, therefore, a catchall term like 'PSD'. However, it at least provides a meaningful description of the relevant physics, whereas the term 'PSD' is misleading at a fundamental level because the origin of magnetic stability in 'PSD' particles is not due to SD-like magnetic moments.

6. Conclusions

Since being proposed by *Stacey* [1961, 1962], the term 'pseudo-single domain' has come to be the prevalent term used to describe the transitional state between the single and multi-domain states in paleomagnetism and rock magnetism. We present evidence from FORC diagrams, micromagnetic simulations, and electron holography to make the case that the 'PSD' state is better described by the vortex state. As particle size increases above the range over which uniform magnetizations occur, flower (Figure 2a) and vortex structures (Figure 2b, c) nucleate. Vortex-like structures, which are observed in all types of magnetic materials [e.g., *Coey*, 2010], are the equilibrium or lowest energy state for non-uniformly magnetized particles in 3D micromagnetic calculations [*Williams and Dunlop*, 1995]. The transition from the stable SD/flower state to the vortex state is sharp, yet magnetic properties through the 'PSD' size range vary gradually. This observation is best reconciled by the fact that materials studied in paleomagnetism and rock magnetism almost always have magnetic particle size and shape distributions, which result in gradual variation of bulk magnetic properties due to the summed responses of millions of magnetic particles. As vortex state particles increase in size, more complex magnetization structures occur, where domain walls nucleate alongside single (Figure 2c, d) or multiple vortex cores, along with less well documented magnetic structures such as antivortices, cross tie walls, and Bloch points. Thus, single vortex states explain the fine end of the 'PSD' particle size range, while domain walls along with single/multiple vortex cores control magnetization structures at the coarser end of the 'PSD' size range. When genuine MD behavior occurs, magnetizations will be dominated by domain wall pinning [*Néel*, 1955; *Pike et al*., 2001]. The persistence of weak but stable remanences and the gradual decline in remanence with increasing particle size through the 'PSD' size range is likely explained by the imbalanced nature of magnetic moments in complex magnetic structures within magnetic particles in the vortex state [*Einsle et al*., 2016]. Available evidence suggests that these structures can record paleomagnetically meaningful information over long geological periods [*Almeida et al*., 2014, 2016; *Nagy et al*., 2017].

Many details of complex magnetization structures across the critical vortex state size range remain to be well understood, but the tools now exist to enable their systematic documentation and understanding. We propose that the term 'vortex state' better describes the physics of the relevant magnetization processes and that the term 'pseudo-single domain' should be abandoned.

Acknowledgements

This paper was improved by the comments of three reviewers, the Associate Editor, and the Editor. We thank Randy Dumas and Alexei Smirnov for providing data that were reprocessed for this paper and the Australian Research Council for financial support through grant DP160100805. Micromagnetic model outputs presented in this paper were produced using MERRILL, the source code of which is publicly available at https://bitbucket.org/wynwilliams/merrill.

References

Almeida, T. P., T. Kasama, A. R. Muxworthy, W. Williams, L. Nagy, T. W. Hansen, P. D. Brown, and R. E. Dunin-Borkowski (2014), Visualized effect of oxidation on magnetic recording fidelity in pseudo-single-domain magnetite particles, *Nat. Commun.*, *5*, 5154, doi:10.1038/ncomms6154.

Almeida, T. P., A. R. Muxworthy, A. Kovács, W. Williams, P. D. Brown, and R. E. Dunin-Borkowski (2016), Direct visualization of the thermomagnetic behavior of pseudo–single-domain magnetite particles, *Sci. Adv.*, *2*, doi:10.1126/sciadv.1501801.

Amin, N., S. Arajs, and E. Matijevic (1987), Magnetic properties of uniform spherical magnetic particles prepared from ferrous hydroxide gels, *Phys. Stat. Sol.*, *101*, 233–238.

Argyle, K. S., and D. J. Dunlop (1990), Low-temperature and high-temperature hysteresis of small multidomain magnetites (215-540 nm), *J. Geophys. Res.*, *95*, 7069–7083.

Banerjee, S. K. (1977), On the origin of stable remanence in pseudo-single domain grains, *Adv. Earth Planet. Sci.*, *1*, 87–97.

Brandt, R., R. Rückreim, D. A. Gilbert, F. Ganss, T. Senn, K. Liu, M. Albrecht, and H. Schmidt (2013), Size-dependent magnetization switching characteristics and spin wave modes of FePt nanostructures, *J. Appl. Phys.*, *113*, 203910, doi:10.1063/1.48079230.

Brown Jr., W. F. (1957), Criterion for uniform micromagnetization, *Phys. Rev.*, *105*, 1479–1482.

Brown Jr., W. F. (1958), Rigorous approach to the theory of ferromagnetic microstructure, *J. Appl. Phys.*, *29*, 470–471.

Bryson, J. F. J., T. Kasama, R. E. Dunin-Borkowski, and R. J. Harrison (2013), Ferrimagnetic/ferroelastic domain interactions in magnetite below the Verwey transition. Part II: Micromagnetic and image simulations, *Phase Transit.*, *86*, 88–102.

Butler, R. F., and S. K. Banerjee (1975), Single-domain grain size limits for metallic iron, *J. Geophys. Res.*, *80*, 252–259.

Carvallo, C., and A. R. Muxworthy (2006), Low-temperature first-order reversal curve (FORC) diagrams for synthetic and natural samples, *Geochem. Geophys. Geosyst.*, *7*, Q09003, doi:10.1029/2006GC001299.

Carvallo, C., A. R. Muxworthy, D. J. Dunlop, and W. Williams (2003), Micromagnetic modeling of first-order reversal curve (FORC) diagrams for single-domain and pseudo-single-domain magnetite, *Earth Planet. Sci. Lett.*, *213*, 375–390.

Chang, L., A. P. Roberts, D. Heslop, A. Hayashida, J. H. Li, X. Zhao, W. Tian, and Q. H. Huang (2016), Widespread occurrence of silicate-hosted magnetic mineral inclusions in marine sediments and their contribution to paleomagnetic recording, *J. Geophys. Res.*, *121*, 8415–8431.

Channell, J. E. T., R. J. Harrison, I. Lascu, I. N. McCave, F. D. Hibbert, and W. E. N. Austin (2016), Magnetic record of deglaciation using FORC-PCA, sortable-silt grain size, and magnetic excursion at 26 ka, from the Rockall Trough (NE Atlantic), *Geochem. Geophys. Geosyst*., *17*, 1823–1841.

Church, N. S. (2010), Magnetic properties of iron-titanium oxides and their nanoscale intergrowths, Ph.D. thesis, University of Cambridge.

Coey, J. M. D. (2010), *Magnetism and Magnetic Materials*, Cambridge Univ. Press, Cambridge, 614 pp.

Cowley, J. M. (1992), Twenty forms of electron holography, *Ultramicroscopy*, *41*, 335–348.

Day, R., M. Fuller, and V. A. Schmidt (1977), Hysteresis properties of titanomagnetites: Grain size and composition dependence, *Phys. Earth Planet. Inter.*, *13*, 260–267.

Dobrota, C. I., and A. Stancu (2013), What does a first-order reversal curve diagram really mean? A study case: Array of ferromagnetic nanowires, *J. Appl. Phys*., *113*, 043928, doi:10.1063/1.4789613.

Donnelly, C., M. Guizar-Sicairos, V. Scagnoli, S. Gliga, M. Holler, J. Raabe, and L. J. Heyderman (2017), Three-dimensional magnetization structures revealed with X-ray vector nanotomography, *Nature*, *547*, 328–331.

Dumas, R. K., C. P. Li, I. V. Roshchin, I. K. Schuller, and K. Liu (2007a), Magnetic fingerprints of sub-100 nm Fe dots, *Phys. Rev. B, 75*, 134405, doi:10.1103/PhysRevB.75.134405.

Dumas, R. K., K. Liu, C. P. Li, I. V. Roshchin, and I. K. Schuller (2007b), Temperature induced single domain-vortex state transition in sub-100 nm Fe nanodots, *Appl. Phys. Lett., 91*, 202501, doi:10.1063/1.2807276.

Dumas, R. K., T. Gredig, C. P. Li, I. K. Schuller, and K. Liu (2009), Angular dependence of vortex-annihilation fields in asymmetric cobalt dots, *Phys. Rev. B, 80*, 014416, doi:10.1103/PhysRevB.80.014416.

Dumas, R. K., C. P. Li, I. V. Roshchin, I. K. Schuller, and K. Liu (2012), Deconvoluting reversal modes in exchange-biased nanodots, *Phys. Rev. B, 86*, 144410, doi:10.1103/PhysRevB.86.144410.

Dunin-Borkowski, R. E., M. R. McCartney, R. B. Frankel, D. A. Bazylinski, M. Pósfai, and P. R. Buseck (1998), Magnetic microstructure of magnetotactic bacteria by electron holography, *Science, 282*, 1868–1870.

Dunlop, D. J. (1973), Superparamagnetic and single domain threshold sizes in magnetite, *J. Geophys. Res., 78*, 1780–1793.

Dunlop, D. J. (1977), The hunting of the 'PSARK', *J. Geomagn. Geoelectr., 29*, 293–318.

Dunlop, D. J. (1981), The rock magnetism of fine particles, *Phys. Earth Planet. Inter., 26*, 1–26.

Dunlop, D. J. (1983), On the demagnetizing energy and demagnetizing factor of a multi-domain ferromagnetic cube, *Geophys. Res. Lett., 10*, 79–82.

Dunlop, D. J. (1986), Hysteresis properties of magnetite and their dependence on particle size: A test of pseudo-single-domain remanence models, *J. Geophys. Res., 91*, 9569–9584.

Dunlop, D. J. (1995), Magnetism in rocks, *J. Geophys. Res., 100*, 2161–2174.

Dunlop, D. J. (2002), Theory and application of the Day plot (M_{rs}/M_s versus H_{cr}/H_c) 1. Theoretical curves and tests using titanomagnetite data, *J. Geophys. Res., 107* (B3), 2056, doi:10.1029/2001JB000486.

Dunlop, D. J., and Ö. Özdemir (1997), *Rock Magnetism*: *Fundamentals and Frontiers*, Cambridge University Press, Cambridge, UK, 573 pp.

Egli, R. (2006), Theoretical aspects of dipolar interactions and their appearance in first-order reversal curves of thermally activated single-domain particles, *J. Geophys. Res.*, *111*, B12S17, doi:10.1029/2006JB004567.

Egli, R., and M. Winklhofer (2014), Recent developments on processing and interpretation aspects of first-order reversal curves (FORC), *Proc. Kazan Univ.*, *156*, 14–53.

Egli, R., A. P. Chen, M. Winklhofer, K. P. Kodama, and C. S. Horng (2010), Detection of noninteracting single domain particles using first-order reversal curve diagrams, *Geochem. Geophys. Geosyst.*, *11*, Q01Z11, doi:10.1029/2009GC002916.

Einsle, J. F., R. J. Harrison, T. Kasama, P. ÓConbhui, K. Fabian, W. Williams, L. Woodland, R. R. Fu, B. P. Weiss, and P. A. Midgley (2016), Multi-scale three-dimensional characterization of iron particles in dusty olivine: Implications for paleomagnetism of chondritic meteorites, *Am. Mineral.*, *101*, 2070–2084.

Enkin, R. J., and D. J. Dunlop (1987), A micromagnetic study of pseudo single-domain remanence in magnetite, *J. Geophys. Res.*, *92*, 12,726–12,740.

Enkin, R. J., and W. Williams (1994), Three-dimensional micromagnetic analysis of stability in fine magnetic grains, *J. Geophys. Res.*, *99*, 611–618.

Evans, M. E., M. W. McElhinny, and A. C. Gifford (1968), Single domain magnetite and high coercivities in a gabbroic intrusion, *Earth Planet. Sci. Lett.*, *4*, 142–146.

Fabian, K. (2003), Some additional parameters to estimate domain state from isothermal remanent magnetization, *Earth Planet. Sci. Lett.*, *213*, 337–345.

Fabian, K., and A. Hubert (1999), Shape-induced pseudo-single domain remanence, *Geophys. J. Int.*, *138*, 717–726.

Fabian, K., A. Kirchner, W. Williams, F. Heider, T. Leibl, and A. Huber (1996), Three-dimensional

micromagnetic calculations for magnetite using FFT, *Geophys. J. Int*., *124*, 89–104.

Feinberg, J. M., R. J. Harrison, T. Kasama, R. E. Dunin-Borkowski, G. R. Scott, and P. R. Renne (2006), Effects of internal mineral structures on the magnetic remanence of silicate-hosted titanomagnetite inclusions: An electron holography study, *J. Geophys. Res*., *111*, B12S15, doi:10.1029/2006JB004498.

Frei, E. H., S. Shtrikman, and D. Treves (1957), Critical size and nucleation field of ideal ferromagnetic particles, *Phys. Rev*., *106*, 446–455.

Fuller, M. (1984), On the grain size dependence of the behaviour of fine magnetic particles in rocks, *Geophys. Surv*., *7*, 75–87.

de Groot, L. V., K. Fabian, I. A. Bakelaar, and M. J. Dekkers (2014), Magnetic force microscopy reveals meta-stable magnetic domain states that prevent reliable absolute palaeointensity experiments, *Nature Comm*., *5*, 4548, doi:10.1038/ncomms5548.

Halgedahl, S. L. (1987), Domain pattern observations in rock magnetism: Progress and problems, *Phys. Earth Planet. Inter*., *46*, 127–163.

Halgedahl, S. L. (1991), Magnetic domain patterns observed on synthetic Ti-rich titanomagnetite as a function of temperature and in states of thermoremanent magnetization, *J. Geophys. Res*., *96*, 3943–3972.

Halgedahl, S., and M. Fuller (1980), Magnetic domain observations of nucleation processes in fine particles of intermediate titanomagnetite, *Nature*, *288*, 70–72.

Halgedahl, S., and M. Fuller (1983), The dependence of magnetic domain structure upon magnetization state with emphasis upon nucleation as a mechanism for pseudo-single-domain behavior, *J. Geophys. Res*., *88*, 6505–6522.

Harada, K., O. Kamimura, H. Kasai, T. Matsuda, A. Tonomura, and V. V. Moshchalkov (1996), Direct observation of vortex dynamics in superconducting films with regular arrays of defects, *Science*, *274*, 1167–1170.

Harrison, R. J., R. E. Dunin-Borkowski, and A. Putnis (2002), Direct imaging of nanoscale magnetic interactions in minerals, *Proc. Natl. Acad. Sci. USA, 99*, 16,556–16,561.

Heider, F., D. J. Dunlop, and N. Sugiura (1987), Magnetic properties of hydrothermally recrystallized magnetite crystals, *Science*, *236*, 1287–1290.

Heider, F., S. L. Halgedahl, and D. J. Dunlop (1988), Temperature dependence of magnetic domains in magnetite crystals, *Geophys. Res. Lett*., *15*, 499–502.

Heider, F., A. Zitzelsberger, and K. Fabian (1996), Magnetic susceptibility and remanent coercive force in grown magnetite crystals from 0.1 μm to 6 mm, *Phys. Earth Planet. Inter*., *93*, 239–256.

Heslop, D., and A. P. Roberts (2012), Estimation of significance levels and confidence intervals for first-order reversal curve distributions, *Geochem. Geophys. Geosyst.*, *13*, Q12Z40, doi:10.1029/2012GC004115.

Ingham, E., G. M. Turner, C. E. Conway, D. Heslop, A. P. Roberts, G. Leonard, D. Townsend, and A. Calvert (2017), Volcanic records of the Laschamp geomagnetic excursion from Mt Ruapehu, New Zealand, *Earth Planet. Sci. Lett.*, *472*, 131–141.

Ivanov, Y. P., A. Chuvilin, L. G. Vivas, J. Kosel, O. Chubykalo-Fesenko, and M. Vázquez (2016), Single crystalline cylindrical nanowires — toward dense 3D arrays of magnetic vortices, *Sci. Rep*., *6*, 23844, doi:10.1038/srep23844.

Kasama, T., R. J. Harrison, N. S. Church, M. Nagao, J. M. Feinberg, and R. E. Dunin-Borkowski (2013), Ferrimagnetic/ferroelastic domain interactions in magnetite below the Verwey transition. Part I: Electron holography and Lorentz microscopy, *Phase Transit*., *86*, 67–87.

Kasama, T., N. S. Church, J. M. Feinberg, R. E. Dunin-Borkowski, and R. J. Harrison (2010), Direct observation of ferrimagnetic/ferroelastic domain interactions in magnetite below the Verwey transition, *Earth Planet. Sci Lett*., *297*, 10–17.

King, J. G., W. Williams, C. D. W. Wilkinson, S. McVitie, and J. N. Chapman (1996), Magnetic properties of magnetite arrays produced by the method of electron beam lithography, *Geophys. Res. Lett*., *23*, 2847–2850.

Krása, D., C. D. W. Wilkinson, N. Gadegaard, X. Kong, H. Zhou, A. P. Roberts, A. R. Muxworthy, and W. Williams (2009), Nanofabrication of two-dimensional arrays of magnetite particles for fundamental rock magnetic studies, *J. Geophys. Res*., *114*, B02104, doi:10.1029/2008JB006017.

Lappe, S.-C. L. L., N. S. Church, T. Kasama, A. Bastos da Silva Fanta, G. Bromiley, R. E. Dunin-Borkowski, J. M. Feinberg, S. Russell, and R. J. Harrison (2011), Mineral magnetism of dusty olivine: A credible recorder of pre-accretionary remanence, *Geochem. Geophys. Geosyst.*, *12*, Q12Z35, doi:10.1029/2011GC003811.

Lappe, S.-C. L. L., J. M. Feinberg, A. Muxworthy, and R. J. Harrison (2013), Comparison and calibration of nonheating paleointensity methods: A case study using dusty olivine, *Geochem. Geophys. Geosyst.*, *14*, 2143–2158.

Lascu, I., R. J. Harrison, Y. Li, J. R. Muraszko, J. E. T. Channell, A. M. Piotrowski, and D. A. Hodell (2015), Magnetic unmixing of first-order reversal curve diagrams using principal component analysis, *Geochem. Geophys. Geosyst*., *16*, 2900–2915.

Levi, S., and R. T. Merrill (1978), Properties of single-domain, pseudo-single-domain, and multi-domain magnetite, *J. Geophys. Res*., *83*, 309–323.

Li, Y. L. (2012), Hexagonal platelet-like magnetite as a biosignature of thermophilic iron-reducing bacteria and its applications to the exploration of the modern deep, hot biosphere and the emergence of iron-reducing bacteria in early Precambrian oceans, *Astrobiology*, *12*, 1100–1108.

Luborsky, F. E. (1961), Development of elongated particle magnets, *J. Appl. Phys*., *32*, S171–S183.

Moskowitz, B. M. (1980), Theoretical grain size limits for single-domain, pseudo-single-domain and multi-domain behavior in titanomagnetite (x = 0.6) as a function of low-temperature oxidation, *Earth Planet. Sci. Lett.*, *47*, 285–293.

Moskowitz, B. M., S. L. Halgedahl, and C. A. Lawson (1988), Magnetic domains on unpolished and polished surfaces of titanium-rich titanomagnetite, *J. Geophys. Res*., *93*, 3372–3386.

Muxworthy, A. R. (2013), The role of magnetic interactions in natural systems, *Astron. Geophys*., *54*, 2.31–2.35, doi:10.1093/astrogeo/att036.

Muxworthy, A. R., and D. J. Dunlop (2002), First-order reversal curve (FORC) diagrams for pseudo-single-domain magnetites at high temperature, *Earth Planet. Sci. Lett.*, *203*, 369–382.

Muxworthy, A. R., and E. McClelland (2000), The causes of low-temperature demagnetization of remanence in multidomain magnetite, *Geophys. J. Int.*, *140*, 115–131.

Muxworthy A. R., and W. Williams (1999), Micromagnetic models of pseudo-single domain grains of magnetite near the Verwey transition, *J. Geophys. Res.*, *104*, 29,203–29,217.

Muxworthy, A. R., and W. Williams (2005), Magnetostatic interaction fields in first-order-reversal curve diagrams, *J. Appl. Phys.*, *97*, 063905, doi:10.1063/1.1861518.

Muxworthy, A. R., and W. Williams (2009), Critical superparamagnetic/single domain grain sizes in interacting magnetite particles: Implications for magnetosome crystals, *J. R. Soc. Interface*, *6*, 1207–1212.

Muxworthy, A. R., and W. Williams (2015), Critical single-domain grain sizes in elongated iron particles: Implications for meteoritic and lunar magnetism, *Geophys. J. Int.*, *202*, 578–583.

Muxworthy, A. R., D. Heslop, and W. Williams (2004), Influence of magnetostatic interactions on first-order-reversal-curve (FORC) diagrams: A micromagnetic approach, *Geophys. J. Int.*, *158*, 888–897.

Muxworthy, A .R., D. Krása, W. Williams, and T. P. Almeida (2014), Paleomagnetic recording fidelity of nonideal magnetic systems, *Geochem. Geophys. Geosyst*., *15*, 2254–2261.

Nagy, L., W. Williams, A. R. Muxworthy, K. Fabian, T. P. Almeida, P. Ó Conbhui, and V. P. Shcherbakov (2017), Stability of equidimensional pseudo-single domain magnetite over billion year time-scales, *Proc. Natl. Acad. Sci. USA*, *xx*, yyy-zzz.

Néel, L. (1949), Théorie du trainage magnétique des ferromagnétiques en grains fin avec application aux terres cuites, *Ann. Géophys*., *5*, 99-136.

Néel, L. (1955), Some theoretical aspects of rock magnetism, *Adv. Phys*., *4*, 191–243.

Newell, A. J. (2005), A high-precision model of first-order reversal curve (FORC) functions for single-domain ferromagnets with uniaxial anisotropy, *Geochem. Geophys. Geosyst., 6*, Q05010, doi:10.1029/2004GC000877.

Newell, A. J., and R. T. Merrill (2000), Nucleation and stability of ferromagnetic states, *J. Geophys. Res*., *105*, 19,377–19,391.

Novosad, V., K. Yu. Guslienko, H. Shima, Y. Otani, K. Fukamichi, N. Kitakami, and Y. Shimada (2001), Nucleation and annihilation of magnetic vortices in sub-micron permalloy dots, *IEEE Trans. Magn*., *MEG-37*, 2088–2090.

Özdemir, Ö., and S. K. Banerjee (1982), A preliminary magnetic study of soil samples from west-central Minnesota, *Earth Planet. Sci. Lett*., *59*, 393–403.

Özdemir, Ö., and D. J. Dunlop (1997), Effects of crystal defects and internal stress on the domain structure and magnetic properties of magnetite, *J. Geophys. Res*., *102*, 20,211–20,224.

Ozima, M., M. Ozima, and S. Akimoto (1964), Low temperature characteristics of remanent magnetization of magnetite–self-reversal and recovery phenomena of remanent magnetization, *J. Geomag. Geoelectr*., *16*, 165–177.

Pike, C., and A. Fernandez (1999), An investigation of magnetic reversal in submicron-scale Co dots using first order reversal curve diagrams, *J. Appl. Phys.*, *85*, 6668–6676.

Pike, C. R., A. P. Roberts, and K. L. Verosub (1999), Characterizing interactions in fine magnetic particle systems using first order reversal curves, *J. Appl. Phys.*, *85*, 6660–6667.

Pike, C. R., A. P. Roberts, M. J. Dekkers, and K. L. Verosub (2001), An investigation of multi-domain hysteresis mechanisms using FORC diagrams, *Phys. Earth Planet. Inter., 126*, 11–25.

Pike, C. R., C. A. Ross, R. T. Scalettar, and G. Zimanyi (2005), First-order reversal curve diagram analysis of a perpendicular nickel nanopillar array, *Phys. Rev. B*, *71*, 134407, doi:10.1103/PhysRevB.71.134407.

Pokhil, T. G., and B. M. Moskowitz (1997), Magnetic domains and domain walls in pseudo-single domain magnetite studied with magnetic force microscopy, *J. Geophys. Res.*, *102*, 22,681–22,694.

Rave, W., K. Fabian, and A. Hubert (1998), Magnetic states of small cubic particles with uniaxial anisotropy, *J. Magn. Magn. Mater.*, *190*, 332–348.

Roberts, A. P., C. R. Pike, and K. L. Verosub (2000), FORC diagrams: A new tool for characterizing the magnetic properties of natural samples, *J. Geophys. Res.*, *105*, 28,461–28,475.

Roberts, A. P., D. Heslop, X. Zhao, and C. R. Pike (2014), Understanding fine magnetic particle systems through use of first-order reversal curve diagrams, *Rev. Geophys.*, *52*, 557–602.

Schabes, M. E., and H. N. Bertram (1988), Magnetization processes in ferromagnetic cubes, *J. Appl. Phys.*, *64*, 1347–1357.

Schmidbauer, E., and N. Schembera (1987), Magnetic hysteresis properties and anhysteretic remanent magnetization of spherical Fe_3O_4 particles in the grain size range 60-160 nm, *Phys. Earth Planet. Inter.*, *46*, 77–83.

Shcherbakov, V. (1978), Theory concerning the magnetic properties of pseudo-single domain grains, *Izv. Earth Phys.*, *14*, 356–362 (English translation).

Smirnov, A. V. (2006), Low-temperature magnetic properties of magnetite using first-order reversal curve analysis: Implications for the pseudo-single domain state, *Geochem. Geophys. Geosyst.*, *7*, Q11011, doi:10.1029/2006GC001397.

Smirnov, A.V. (2007), Effect of the magnetic field applied during cooling on magnetic hysteresis in the low-temperature phase of magnetite: First-order reversal curve (FORC) analysis, *Geochem. Geophys. Geosyst.*, *8*, Q08005, doi:10.1029/2007GC001650.

Soffel, H. C. (1977), Domain structure of titanomagnetites and its variation with temperature, *J. Geomag. Geoelectr*., *29*, 277–284.

Stacey, F. D. (1961), Theory of the magnetic properties of igneous rocks in alternating fields, *Philos. Mag*., *6*, 1241–1260.

Stacey, F. D. (1962), A generalized theory of thermoremanence, covering the transition from single domain to multi-domain magnetic grains, *Philos. Mag*., *7*, 1887–1900.

Stacey, F. D. (1963), The physical theory of rock magnetism, *Adv. Phys.*, *12*, 45–133.

Stoner, E. C., and E. P. Wohlfarth (1948), A mechanism of magnetic hysteresis in heterogeneous alloys, *Philos. Trans. R. Soc. Lond.*, *A240*, 599–642.

Tauxe, L., H. N. Bertram, and C. Seberino (2002), Physical interpretation of hysteresis loops: Micromagnetic modeling of fine particle magnetite, *Geochem. Geophys. Geosyst.*, *3*, 1055, doi:10.1029/2001GC000241.

Verhoogen, J. (1959), The origin of thermoremanent magnetization, *J. Geophys. Res*., *64*, 2441–2449.

Verwey, E. J. W. (1939), Electronic conduction of magnetite (Fe_3O_4) and its transition point at low temperatures, *Nature*, *144*, 327–328.

Vlag, P., P. Rochette, and M. J. Dekkers (1996), Some additional hysteresis parameters for a natural (titano)magnetite with known grain size, *Geophys. Res. Lett*., *23*, 2803–2806.

Williams, W., and D. J. Dunlop (1989), Three-dimensional micromagnetic modelling of ferromagnetic domain structure, *Nature*, *337*, 634–637.

Williams, W., and D. J. Dunlop (1995), Simulation of magnetic hysteresis in pseudo-single-domain grains of magnetite, *J. Geophys. Res.*, *100*, 3859–3871.

Williams, W., V. Hoffmann, F. Heider, T. Göddenhenrich, and C. Heiden (1992), Magnetic force microscopy imaging of domain walls in magnetite, *Geophys. J. Int*., *111*, 417–423.

Winklhofer, M., and G. T. Zimanyi (2006), Extracting the intrinsic switching field distribution in perpendicular media: A comparative analysis, *J. Appl. Phys.*, *99*, 08E710, doi:10.1063/1.2176598.

Winklhofer, M., R. K. Dumas, and K. Liu (2008), Identifying reversible and irreversible magnetization changes in prototype patterned media using first- and second-order reversal curves, *J. Appl. Phys.*, *103*, 07C518, doi:10.1063/1.2837888.

Worm, H.-U., and H. Markert (1987), Magnetic hysteresis properties of fine particle titanomagnetites precipitated in a silicate matrix, *Phys. Earth Planet. Inter*., *46*, 84–92.

Yu, Y., and L. Tauxe (2005), On the use of magnetic transient hysteresis in paleomagnetism for granulometry, *Geochem. Geophys. Geosyst.*, *6*, Q01H14, doi:10.1029/2004GC000839.

Xu, S., and D. J. Dunlop (1993), Theory of alternating field demagnetization of multidomain grains and implications for the origin of pseudo-single-domain remanence, *J. Geophys. Res.*, *98*, 4183–4190.

Zhao, X., A. P. Roberts, D. Heslop, G. A. Paterson, Y. L. Li, and J. H. Li (2017), Magnetic domain state diagnosis using hysteresis reversal curves, *J. Geophys. Res.*, *122*, doi:10.1002/2016JB013683.

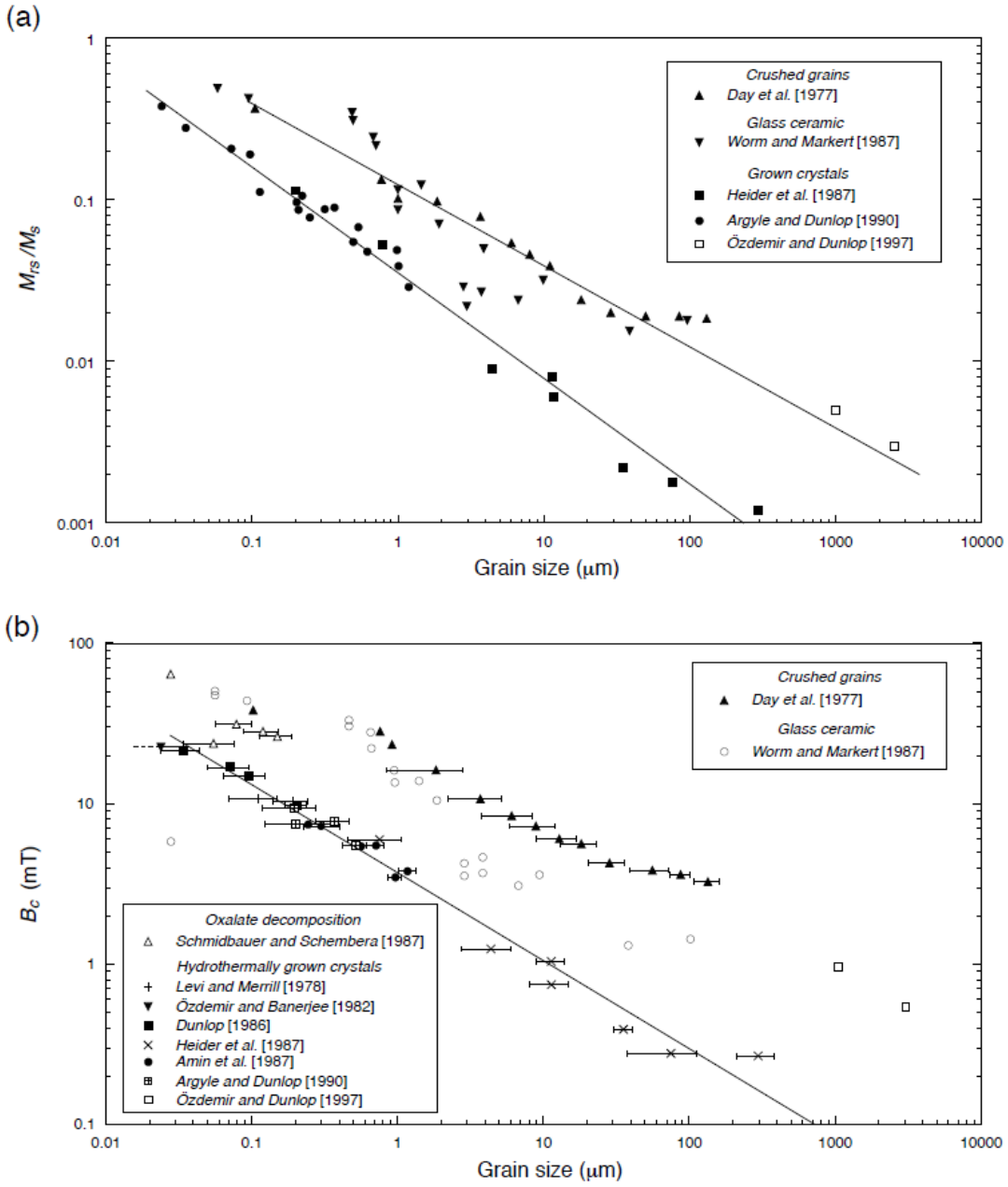

Figure 1 Illustration of the gradual rather than sharp change in magnetic properties for magnetite with increasing grain size, which has been attributed to 'pseudo-single domain' behavior. (a) Plot of M_{rs}/M_s versus grain size (after *Dunlop* [1995] who synthesized data from *Day et al*. [1977], *Worm and Markert* [1987], *Heider et al*. [1987], *Argyle and Dunlop* [1990] and *Özdemir and Dunlop* [1997]), and (b) B_c versus grain size (after *Dunlop and Özdemir* [1997] who synthesized data from *Day et al*. [1977], *Worm and Markert* [1987], *Schmidbauer and Schembera* [1987], *Levi and Merrill* [1978], *Özdemir and Banerjee* [1982], *Dunlop* [1986], *Heider et al*. [1987], *Amin et al.*

[1987], *Argyle and Dunlop* [1990], and *Özdemir and Dunlop* [1997]). The "harder" magnetic properties in crushed magnetite are attributed to the higher state of internal stress compared to the hydrothermally grown or glass ceramic crystals.

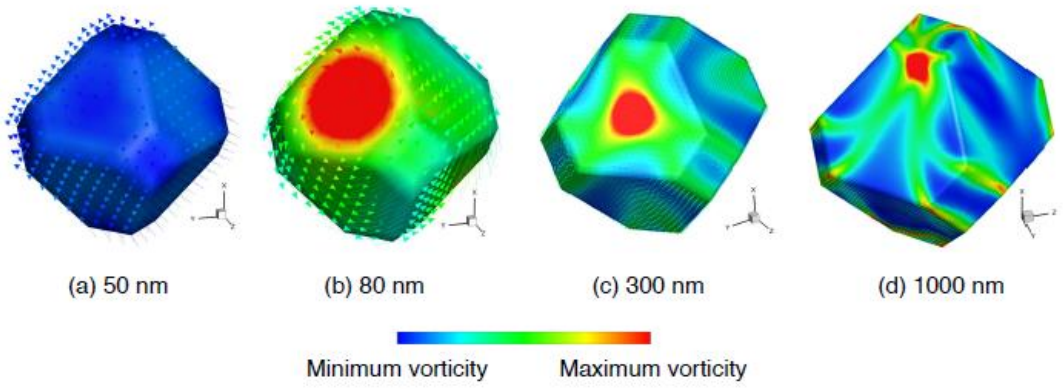

Figure 2 Micromagnetic simulations of magnetic domain structures in cubo-octahedral magnetite grains with progressively increasing size (after *Muxworthy* [2013]). (a) A 50 nm particle in the SD flower state has a uniform magnetic structure in its center with magnetic moments that spread outward at the edges of the particle. (b) At 80 nm, a vortex state spontaneously nucleates. The vortex state persists over a large size range along with coexisting domain walls ((c) 300 nm, (d) 1 μm). Magnetizations are colored according to vorticity, which highlights non-uniform micromagnetic structures.

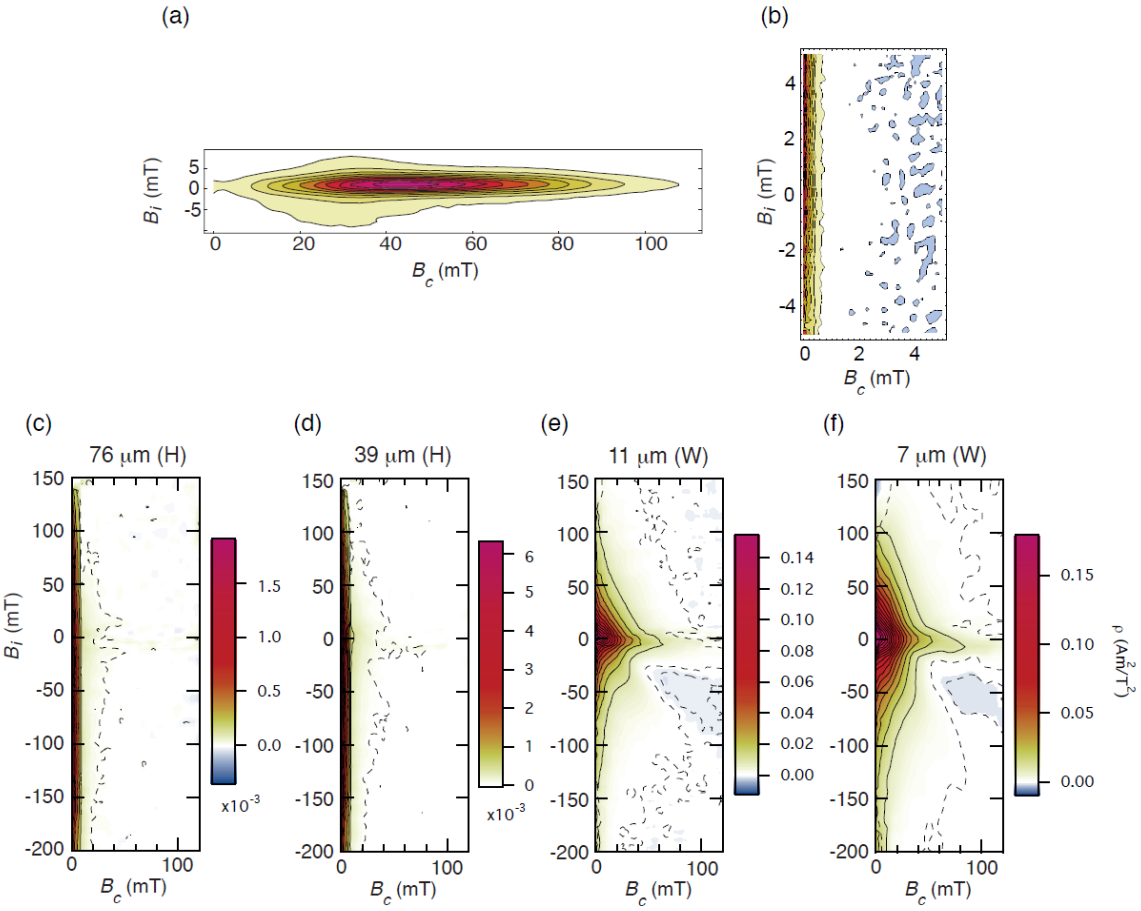

Figure 3 Illustration of the contrasting manifestations of different magnetic domain states on experimental FORC diagrams. (a) Sample CS911 from the Tiva Canyon Tuff, Nevada (after *Roberts et al*. [2000]). The tight distribution of contours along the B_i = 0 axis reflects the non-interacting uniaxial SD nature of the particle assemblage, while the distribution along the B_c axis reflects its coercivity distribution. (b) Transformer steel sample M-80 (after *Pike et al*. [2001]). The vertical FORC distribution centered near B_c = 0 is characteristic of MD particle systems with weak domain wall pinning. Experimental FORC diagrams for a series of synthetic magnetites (H = hydrothermal; W = Wright Industries) with grain size of: (c) 76 μm (H), (d) 39 μm (H), (e) 11 μm (W), and (f) 7 μm (W) (after *Muxworthy and Dunlop* [2002]). With decreasing grain size, FORC distributions progressively diverge away from the vertical distributions expected for MD particle systems (b). We argue in this paper that the divergence is due to coexisting magnetic vortex states.

The dashed lines in (c-f) are 0.05 significance levels for the FORC distributions calculated following *Heslop and Roberts* [2012].

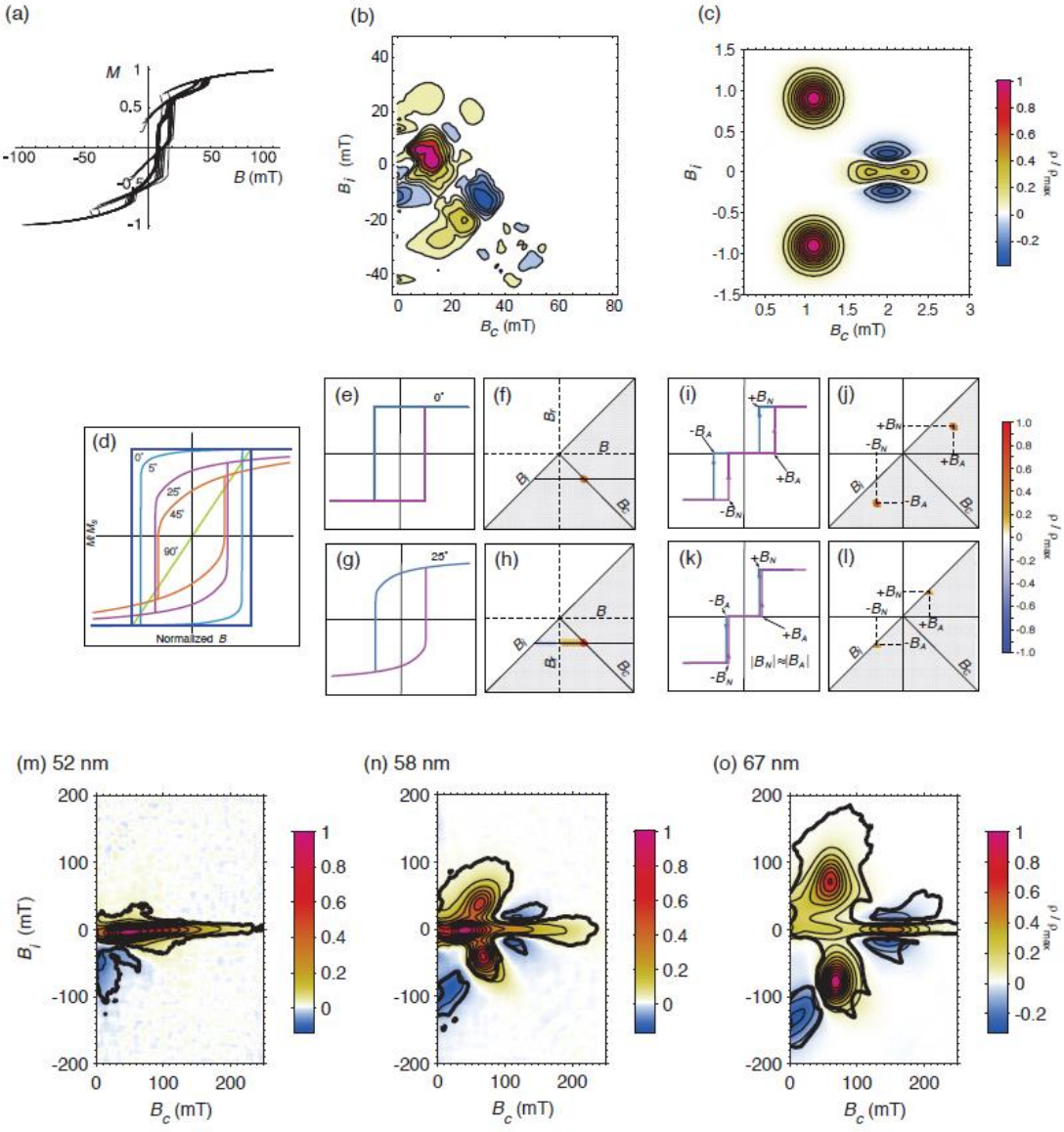

Figure 4 Micromagnetic and numerical simulations, and experimental results for synthetic samples with magnetizations dominated by single vortex nucleation/annihilation. (a, b) Micromagnetic results for an elongated single isolated magnetite particle (100 x 80 x 80 nm) that exceeds the stable SD threshold size. (a) Simulated FORCs indicate changes from the stable SD state with decreasing field from positive saturation to a flower state to a vortex state and back with approach to positive saturation. Magnetization switching events at different fields produce (b) a complex FORC diagram with multiple peaks (after *Carvallo et al*. [2003]). (c) Model results (after *Pike and Fernandez* [1999]) where the offset of the upper and lower peaks from the B_i = 0 axis

provides a measure of the vortex nucleation/annihilation field. The "butterfly" feature on the right-hand side results from the presence of two distinct annihilation fields [*Pike and Fernandez*, 1999] and is not always observed in single vortex systems. (d) Illustration of hysteresis loops for uniaxial SD particles with easy axes at different angles with respect to the applied field (from *Stoner and Wohlfarth* [1948]). (e) Hysteron for an isolated uniaxial SD particle with easy axis parallel to the applied field, and (f) its response on a FORC diagram. (g) Hysteresis loop for a Stoner-Wohlfarth particle oriented 25° to the applied field direction, and (h) its non-singular response with strong positive and weak negative regions on a FORC diagram (see *Muxworthy et al*. [2004], *Newell* [2005], or *Roberts et al*. [2014] for details). (i) Split hysteron representation of a magnetic vortex state (following *Pike and Fernandez* [1999]), where B_N is the vortex nucleation field and B_A is the annihilation field. (j) FORC diagram for such a split hysteron with positive peaks in both the upper and lower FORC half-planes, where the distance of peaks from the B_c axis is a measure of the strength of B_N and B_A, and their distance from the B_i axis is a measure of coercivity (hysteron width), as illustrated for a coarser-grained lower coercivity vortex state in (k) and (l). (d-l) From *Zhao et al*. [2017]. (m-o) FORC diagrams for iron nanodots with progression from (m) stable SD behavior (for 52 nm nanodots) to (n) single vortex behavior (for 58 nm nanodots) to (o) single vortex behavior with a larger nucleation/annihilation field (for 67 nm nanodots; after *Dumas et al*. [2007a]). In (m-o), the thick black lines denote 0.05 significance levels calculated following *Heslop and Roberts* [2012].

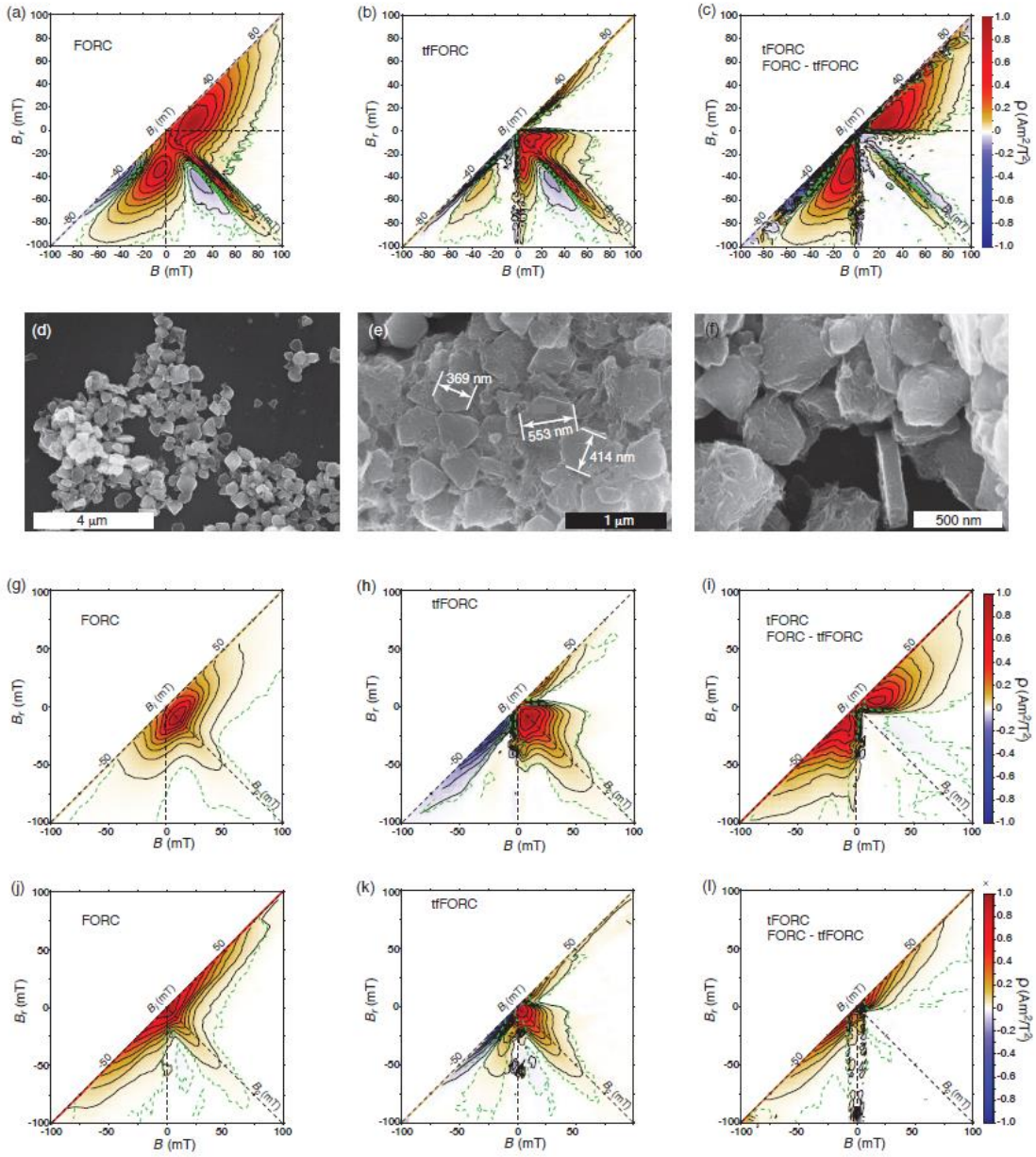

Figure 5 FORC diagrams and scanning electron microscope (SEM) images for hexagonal magnetite plates up to several hundred nm across [*Li*, 2012] with vortex magnetic behavior. (a) Conventional FORC, (b) transient-free FORC (tfFORC), and (c) transient FORC (tFORC (= FORC – tfFORC)) diagrams. (d-f) SEM images of hexagonal magnetite plates [*Li*, 2012] for which FORC diagrams are shown in (a-c). (g-i) The same progression of FORC diagrams as in (a-c) for a typical 'PSD' sample (andesite from Mt Ruapehu, New Zealand; *Ingham et al*. [2017]). (j-l) The same progression of FORC diagrams as in (a-c) for a 120-μm natural MD magnetite. The FORC

diagrams are from *Zhao et al*. [2017], where dashed green lines represent 0.05 significance levels calculated following *Heslop and Roberts* [2012].

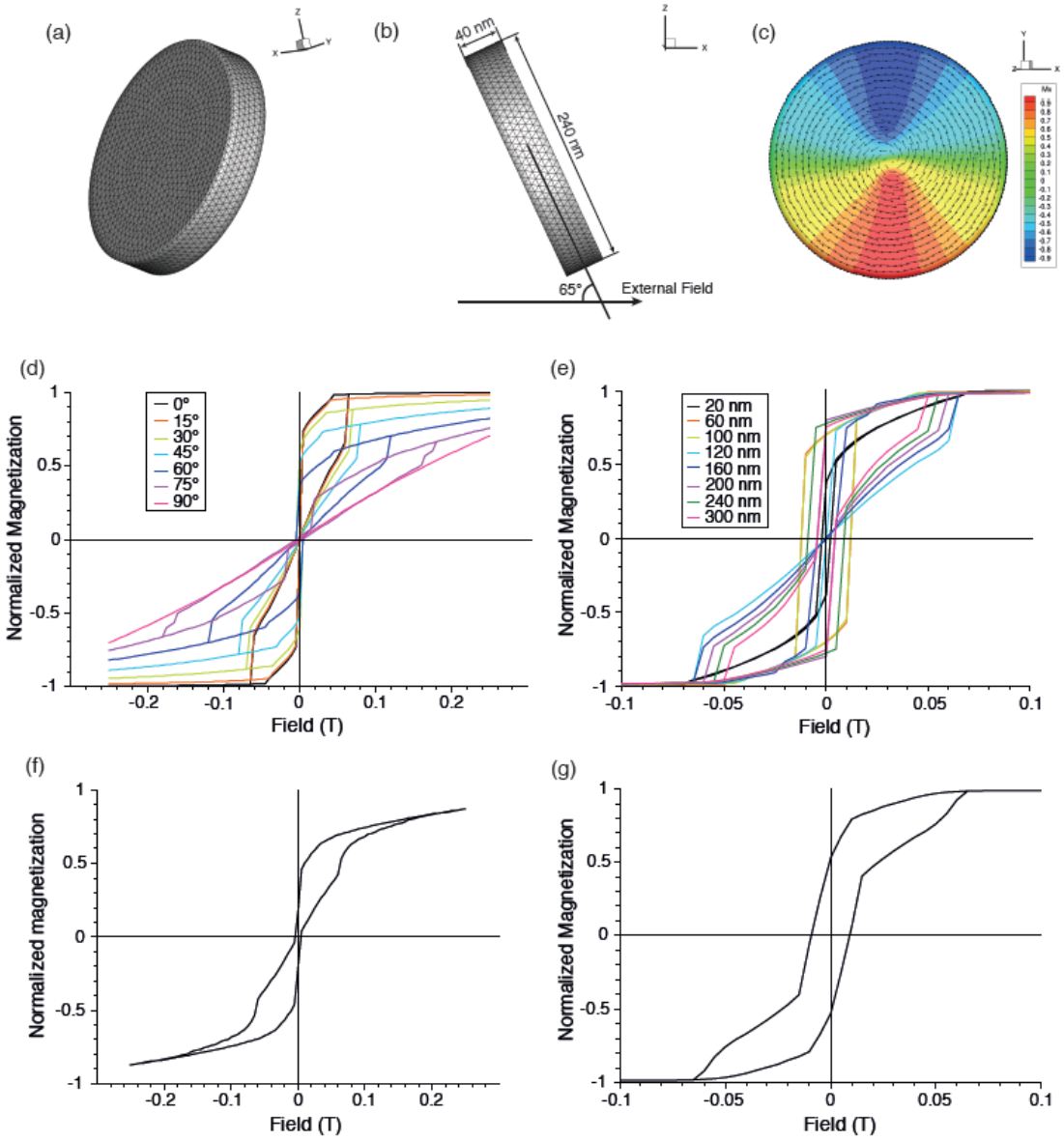

Figure 6 Numerical micromagnetic simulations of hysteresis loops for magnetic particle systems dominated by single vortex nucleation/annihilation. (a) Circular magnetite disk (240 x 40 nm) with finite element mesh used for the simulation. (b) Side-on view of the disk with relationship between applied field angle and the disk. (c) Micromagnetic simulation of the remanence state of the disk when the field is applied parallel to its easy axis (0°). Results of micromagnetic simulations of hysteresis loops for the disk for (d) variable applied field angle (calculated at 5° increments, but shown at 15° increments), and (e) variable disk diameter (from 20 nm to 320 nm). Hysteresis loops for the sum of the (f) 19 angles, and (g) 16 disk diameters illustrate the smoothing that occurs in

real samples with mixed particle sizes and easy axis orientations. For the millions of particles in a typical paleomagnetic sample, smooth loops will result and steps due to vortex nucleation/annihilation will not be evident. The parameters used are for magnetite at 20°C as implemented in MERRILL.

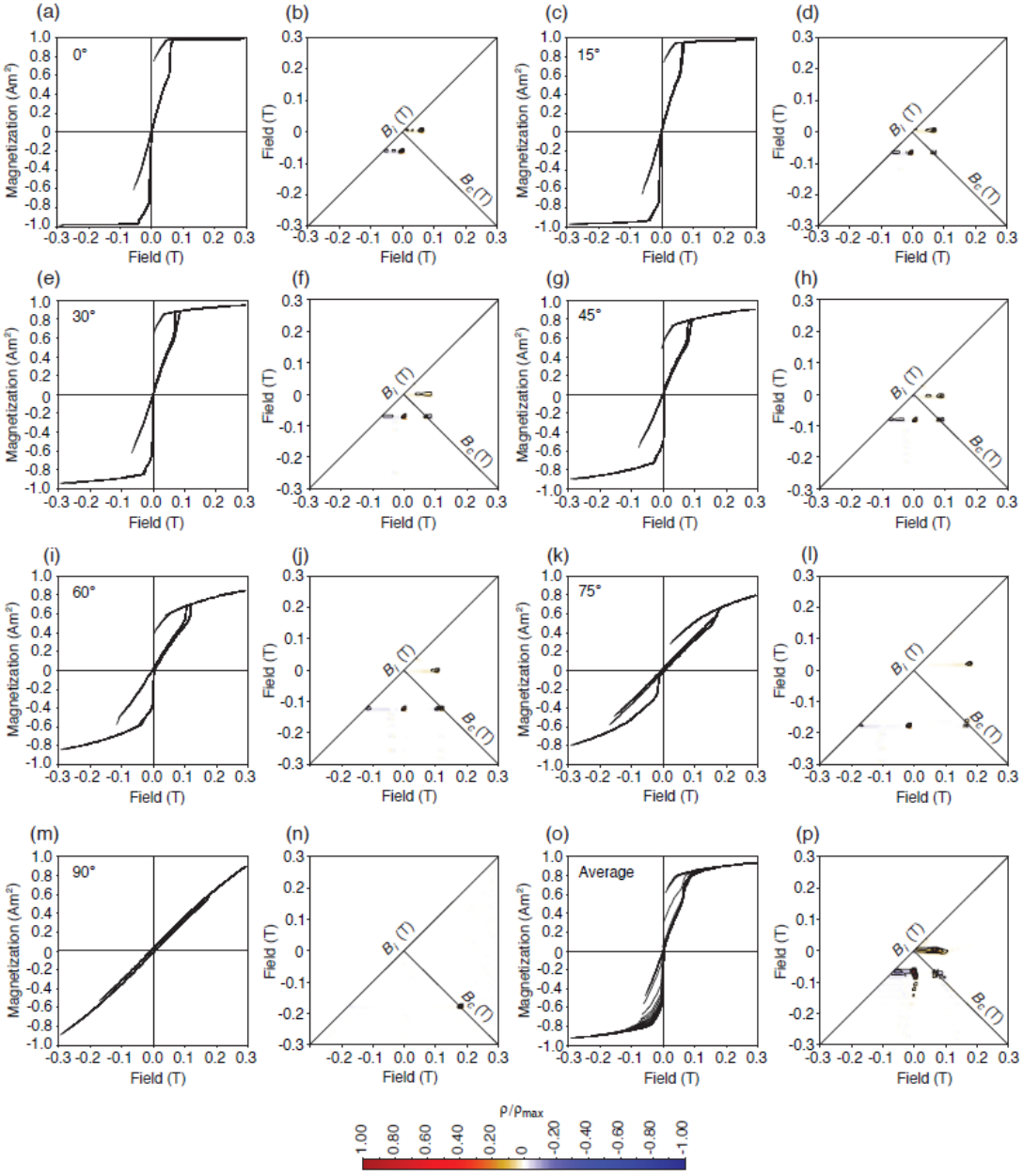

Figure 7 Numerically simulated FORC diagrams for a 240 x 40 nm circular magnetite disk (Figure 6a) that is dominated by single vortex nucleation/annihilation. Pairs of simulated FORCs and conventional FORC diagrams for a range of applied field angles with respect to the magnetization easy axis: (a, b) 0°, (c, d) 15°, (e, f) 30°, (g, h) 45°, (i, j) 60°, (k, l) 75°, (m, n) 90°, and (o, p) the average of 19 simulated angles (at 5° increments). For all cases except the 90° case, a pair of peaks is evident above and below the $B_i = 0$ line, as expected for the vortex state (cf. Figure 4c). For the 90° case, a SD peak is evident.

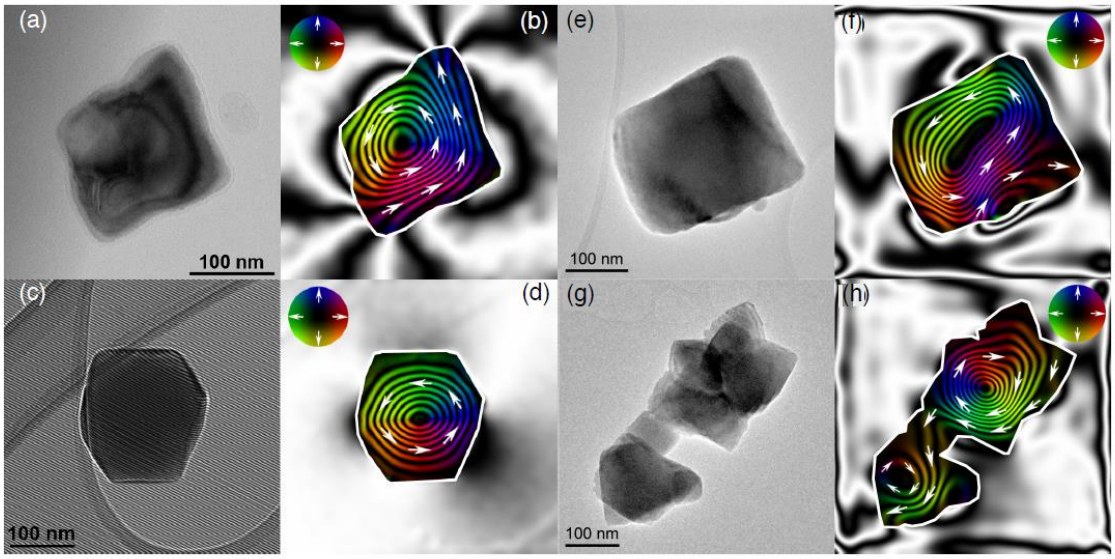

Figure 8 Electron holographic visualizations of single magnetic vortices in magnetite. (a) Bright-field TEM image of a particle ~250 nm in length. (b) Magnetic induction map reconstructed from electron holograms at room temperature (an in-plane saturating field was applied along the particle long-axis to induce a remanent magnetization). (c, d) Electron hologram (with interference fringes used to calculate the magnetic contribution to the phase shift) and magnetic induction map for a hexagonal vortex state particle. Bright-field TEM image and induction map for a: (e, f) single particle and (g, h) cluster of particles with non-vertically aligned vortex cores. All images are from the work of *Almeida et al*. [2016]. The contour spacings (in radians) in the magnetic induction maps are: (b) 0.53, (d) 0.78, (f) 0.39, and (h) 0.53; magnetization directions are indicated with arrows (depicted in the color wheels).

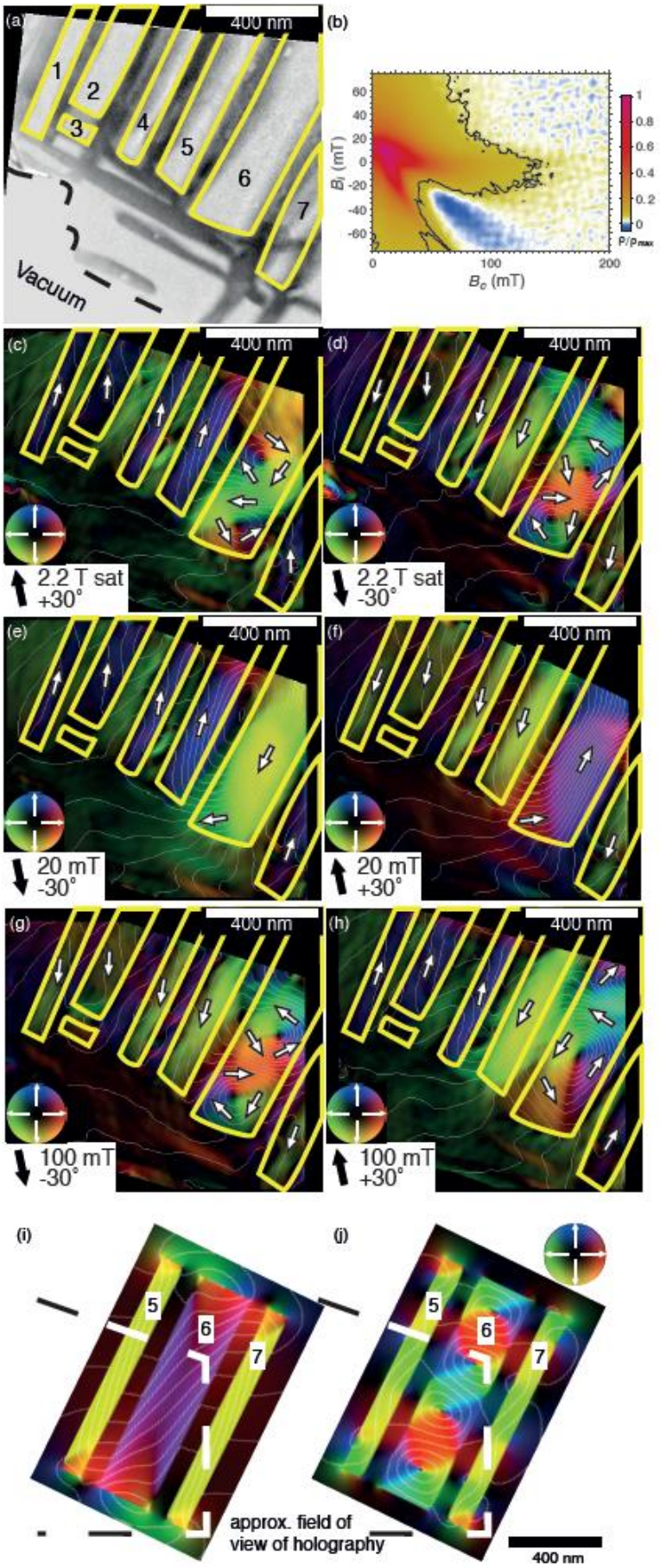

Figure 9 Electron holographic visualizations of multiple vortex states in titanohematite lamellae with FORC results and micromagnetic simulations. (a) Back-scattered SEM image of magnetite laths (1-7) separated by titanohematite lamellae [*Church*, 2010]. The nearly pure magnetite laths and paramagnetic titanohematite lamellae ($Fe_{1.16}Ti_{0.84}O_3$) were produced synthetically by oxy-exsolution of an original titanomagnetite ($Fe_{2.4}Ti_{0.6}O_4$). (b) Conventional FORC diagram, which is typical of bulk 'PSD' behavior (SF = 2), where the black line represents the 0.05 significance level calculated following *Heslop and Roberts* [2012]. (c-h) Magnetic induction maps reconstructed from room-temperature electron holograms (in-plane fields were applied parallel to the black arrow in each image to induce the remanent magnetization represented in each induction map). The contour spacing is 0.53 rad for all induction maps; magnetization directions are indicated with arrows (depicted in the color wheels). The widest (~300 nm) magnetite lath 6 occurs in either a nearly uniformly magnetized state (e, f) or with a series of multiple stable vortices (c, d, g, and h) depending on applied field. (i, j) Micromagnetic simulations conducted with a finite difference algorithm with regular grid points indicate that magnetization switching occurs by nucleation of a vortex that sweeps down the lath. Continuous magnetic flux lines between laths indicate strong magnetic interactions.

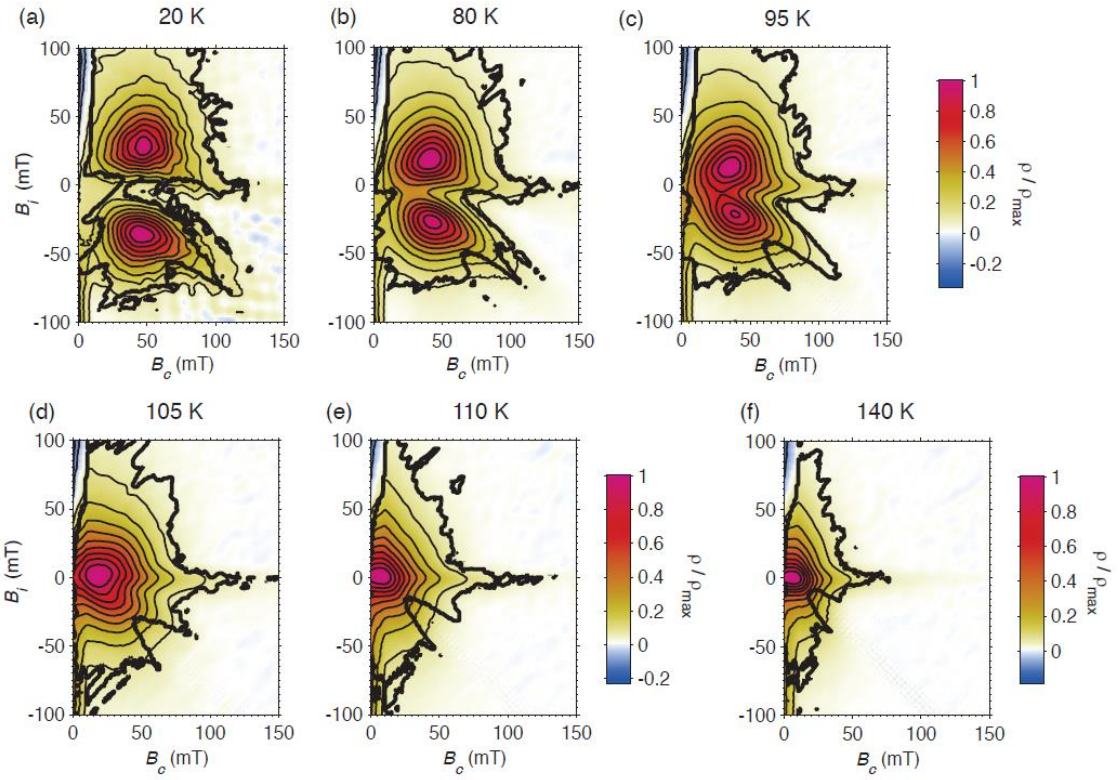

Figure 10 Temperature-dependent FORC diagrams for 'PSD' magnetite above and below the Verwey transition temperature. FORC diagrams (smoothing factor (SF) = 2 for all) measured after zero field cooling during warming from 20 to 140 K at (a) 20 K, (b) 80 K, (c) 95 K, (d) 105 K, (e) 110 K, and (f) 140 K (from *Smirnov* [2006]). Above the Verwey transition temperature, FORC diagrams are typical of 'PSD' particle systems (e.g., Figure 3f). Below the transition, the FORC distributions split into upper and lower peaks, which resemble those for single vortex systems (Figure 4), but without a "butterfly" feature. The thick black lines represent 0.05 significance levels calculated following *Heslop and Roberts* [2012].